Supporting Information

Azo and imine functionalized 2-naphthols: Promising supramolecular gelators for selective detection of Fe^{3+} and Cu^{2+}, reactive oxygen species and halides

Atanu Panja and Kumaresh Ghosh*

Department of Chemistry, University of Kalyani, Kalyani-741235, India.
Email: ghosh_k2003@yahoo.co.in

Table 1S. Results of gelation test for compounds **1-3**.

Solvent	**1**	**2**	**3**
DMSO	S	S	S
DMF	S	S	S
Ethanol	G	G	G
CH_3CN	G	G	S
THF	S	S	S
$CHCl_3$	S	S	S
Petroleum ether	I	I	I
Hexane	I	I	I
2% MeOH in $CHCl_3$	S	S	S
DMSO: H_2O (1:1, v/v)	G (12 mg/mL)	G (10 mg/mL)	G (11 mg/mL)
DMF: H_2O (1:1, v/v)	G (13 mg/mL)	G (11 mg/mL)	G (12 mg/mL)
Ethanol: H_2O (1:1, v/v)	G (17 mg/mL)	G (14 mg/mL)	G (14 mg/mL)
CH_3CN: H_2O (1:1, v/v)	G (9 mg/mL)	G (8 mg/mL)	P
THF: H_2O (1:1, v/v)	S	G (16 mg/mL)	G (18 mg/mL)
S = Solution; G = Gel (mgc); I = Insoluble; P = Precipitation.			

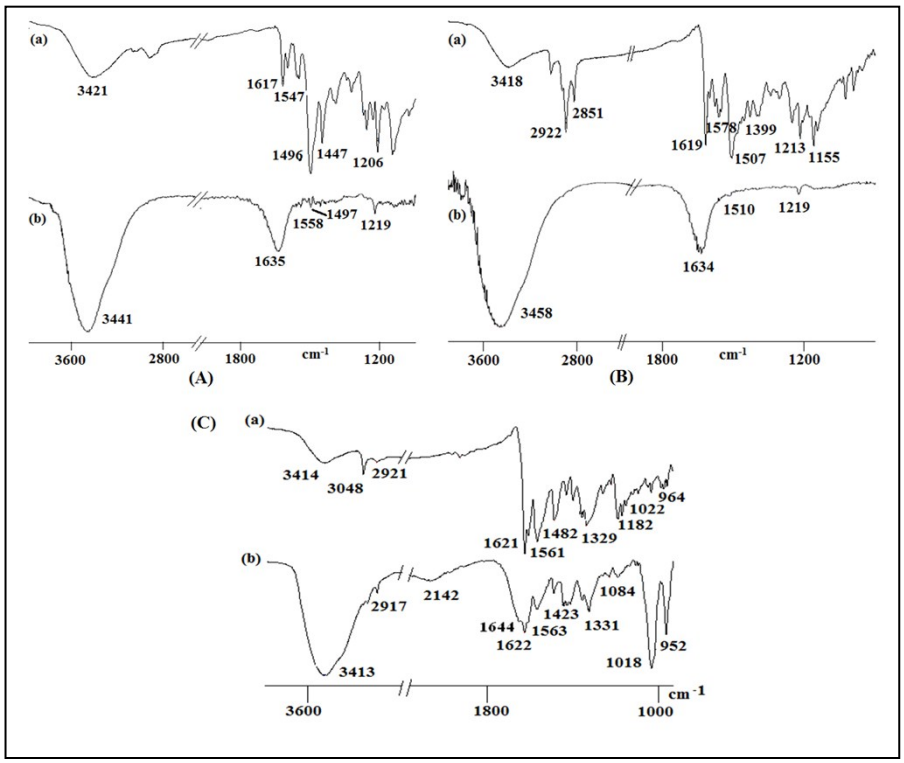

Fig. 1S. Partial FTIR spectra of (A) **1**, (B) **2** and (C) **3** in (a) amorphous (b) gel state.

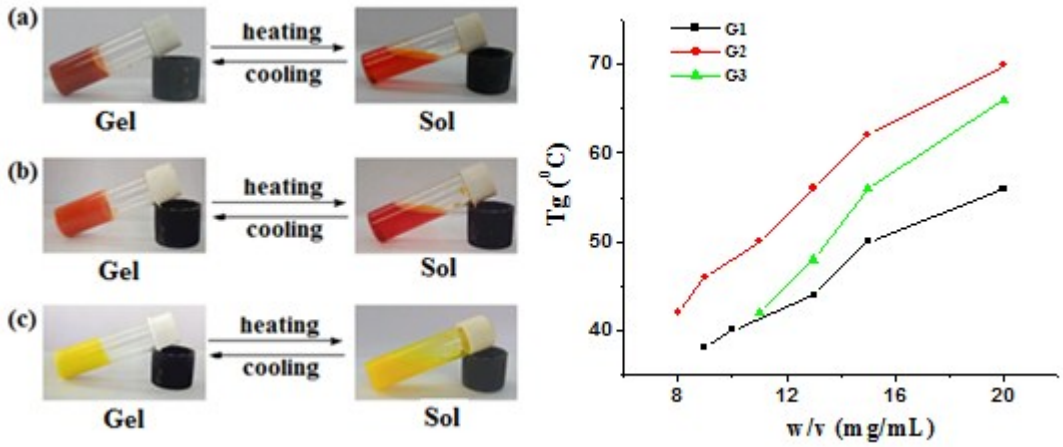

Fig. 2S. Pictorial representation of the thermo reversibility of the CH_3CN: H_2O (1:1, v/v) gel of (a) **1**, (b) **2** and (c) DMSO: H_2O (1:1, v/v) gel of **3** (left) and variation of gel melting temperature (T_g) with increasing concentration of gelators (right).

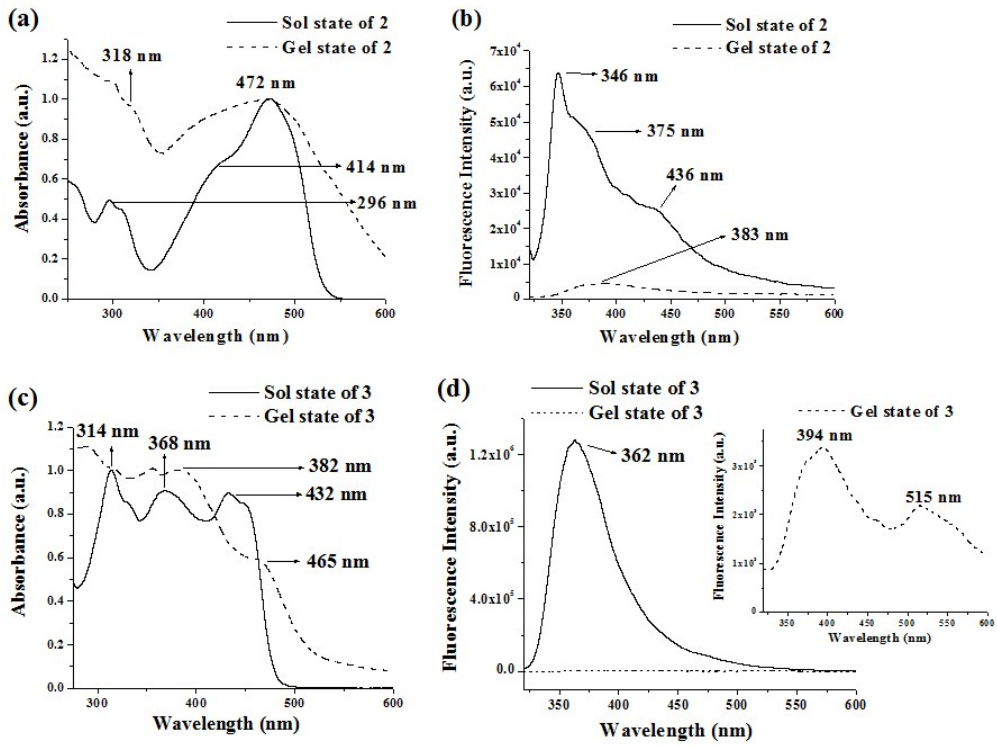

Fig. 3S. Comparison of normalized UV–vis and fluorescence spectra (λex = 310 nm) of **2** (a, b) and **3** (c, d) in the sol and gel states, respectively.

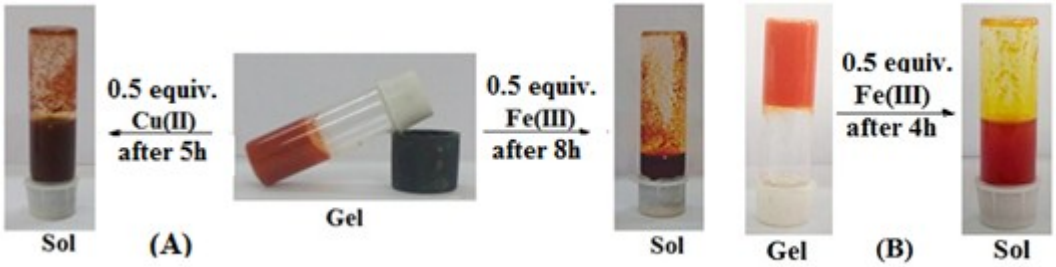

Gelator	Metal ion	Conc. (M)	Equiv.	status
1 (9 mg in 0.5 mL CH_3CN)	Cu^{2+}/Fe^{3+} (0.5 mL in H_2O)	0.2	2.76	Sol
		0.1	1.38	Sol
		0.03	0.41	Sol
		0.02	0.28	Sol
		0.01	0.14	Gel

Gelator	Metal ion	Conc. (M)	Equiv.	status
2 (8 mg in 0.5 mL CH_3CN)	Fe^{3+} (0.5 mL in H_2O)	0.05	0.78	Sol
		0.03	0.47	Sol
		0.02	0.31	Gel

Fig. 4S. Photograph and table representing the sensitivity of the CH_3CN: H_2O (1:1, v/v) gel of (A) **1** and (B) **2** towards Cu^{2+} and Fe^{3+} ions.

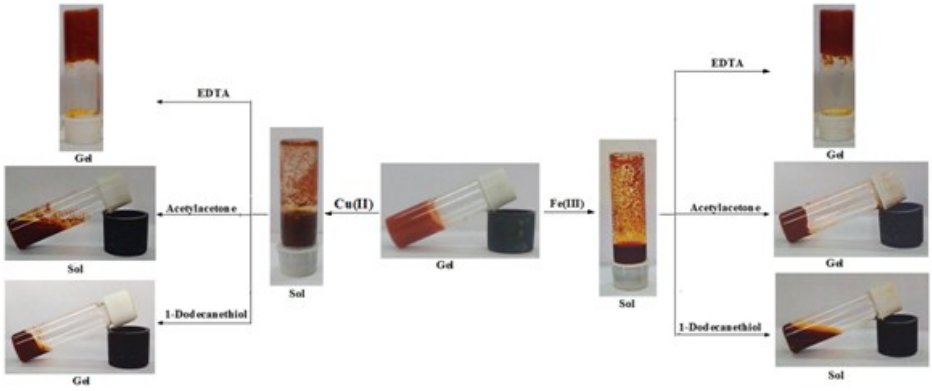

Fig. 5S. Chemical responsiveness of the Cu^{2+} and Fe^{3+} induced broken gel of **1** upon addition of EDTA, acetylacetone and 1-dodecanethiol.

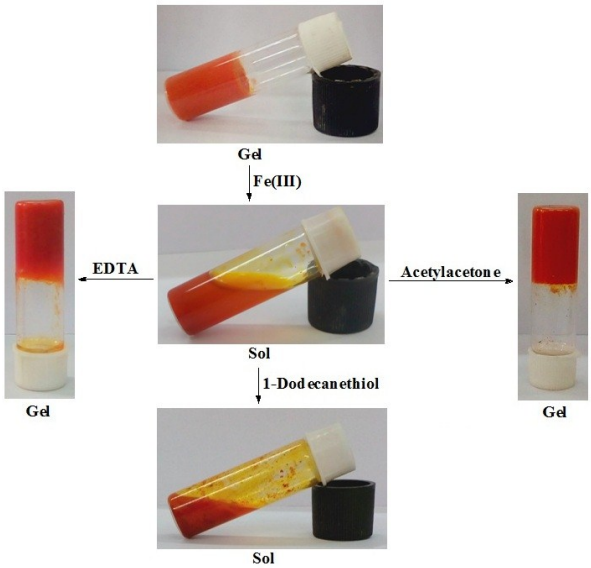

Fig. 6S. Chemical responsiveness of Fe^{3+} induced broken gel of **2** upon addition of EDTA, acetylacetone and 1-dodecanethiol .

.

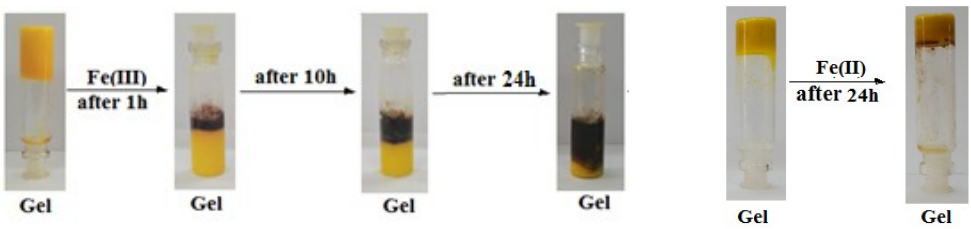

Fig. 7S. Photograph showing the response of the DMSO: H_2O (1:1, v/v) gel of **3** towards Fe^{3+} and Fe^{2+} ions with time upon addition of 1 equiv. amount of said metal ion (c = 0.2 M).

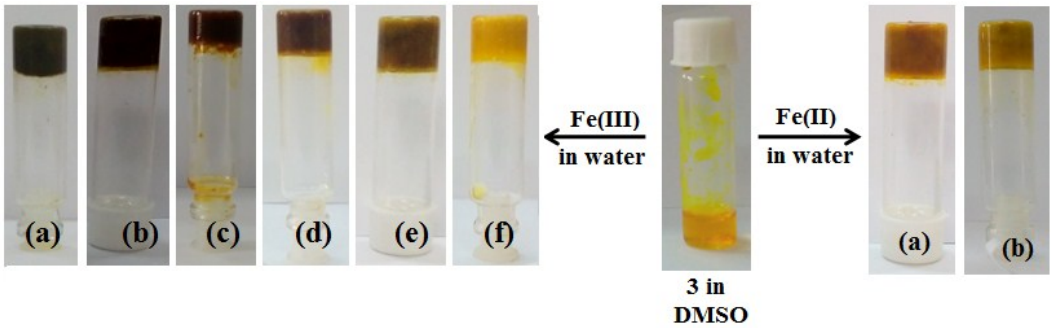

Gelator	Metal ion	Entry	Conc. (M)	Equiv.	Gel color
3 (11 mg in 0.5 mL DMSO)	Fe^{3+} (0.5 mL in H_2O)	(a)	0.03	0.34	Dark brown
		(b)	0.01	0.11	Dark brown
		(c)	0.005	0.06	Dark brown
		(d)	0.003	0.03	Dark brown
		(e)	0.002	0.02	brown
		(f)	0.001	0.01	yellow

Gelator	Metal ion	Entry	Conc. (M)	Equiv.	Gel color
3 (11 mg in 0.5 mL DMSO)	Fe^{2+} (0.5 mL in H_2O)	(a)	0.03	0.34	Brownish yellow
		(b)	0.01	0.11	yellow

Fig.8S. Photograph representing the sensitivity of the gelator towards Fe^{3+} and Fe^{2+} ions.

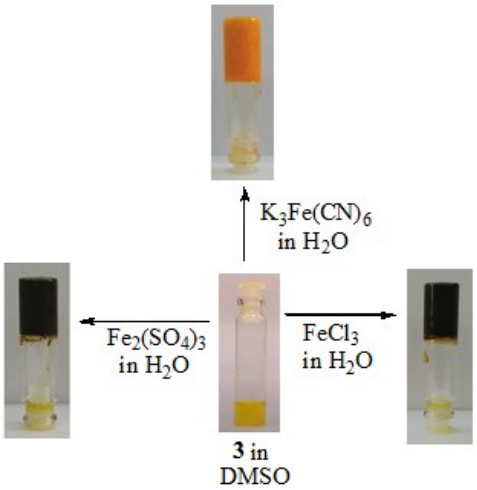

Fig. 9S. Preparation of DMSO-H_2O gel of **3** in presence of $FeCl_3$, $Fe_2(SO_4)_3$ and $K_3Fe(CN)_6$.

Fig. 10S. Chemical responsiveness of Fe^{3+} induced colored gel of **3** upon addition of EDTA and acetylacetone.

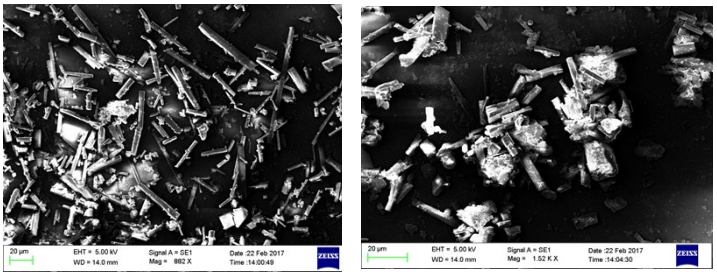

Fig. 11S. SEM images of xerogel of **3** with Fe^{3+} in DMSO: H_2O (1:1, v/v).

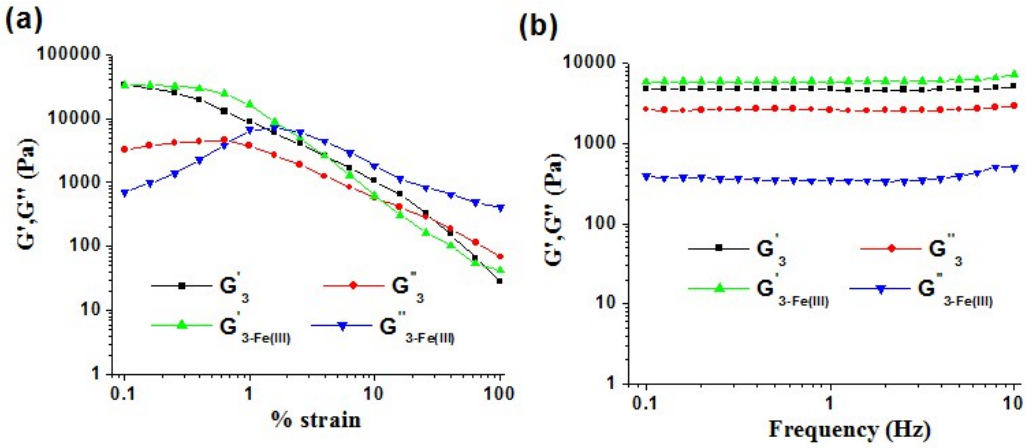

Compound (15 mg/mL with 1 equiv. of Fe^{3+})	Critical strain (%)	G'_{av} (Pa)	G''_{av} (Pa)	(G'_{av}/ $''_{av}$)	tan δ (G''_{av}/ G'_{av})
3-Fe(III)	1.99	6086	376	16.18	0.06

Fig. 12S. Rheological study of the **3**-Fe^{3+} gel; (a) frequency sweep and (b) strain sweep experiments.

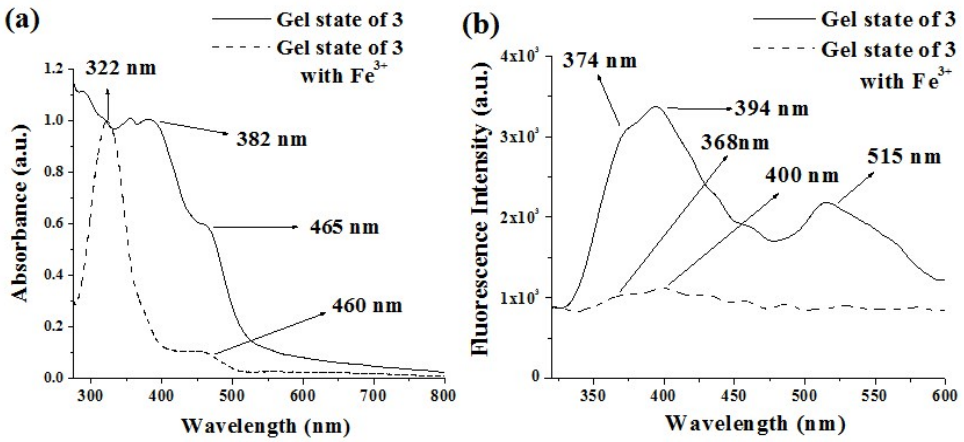

Fig. 13S. Comparison of (a) normalized UV–vis and (b) fluorescence spectra (λex = 310 nm) of gel state of **3** [in DMSO: H_2O (1:1, v/v)] in absence and in presence of Fe^{3+} ion.

FTIR spectra of the metal-ligand complexes of 1-3

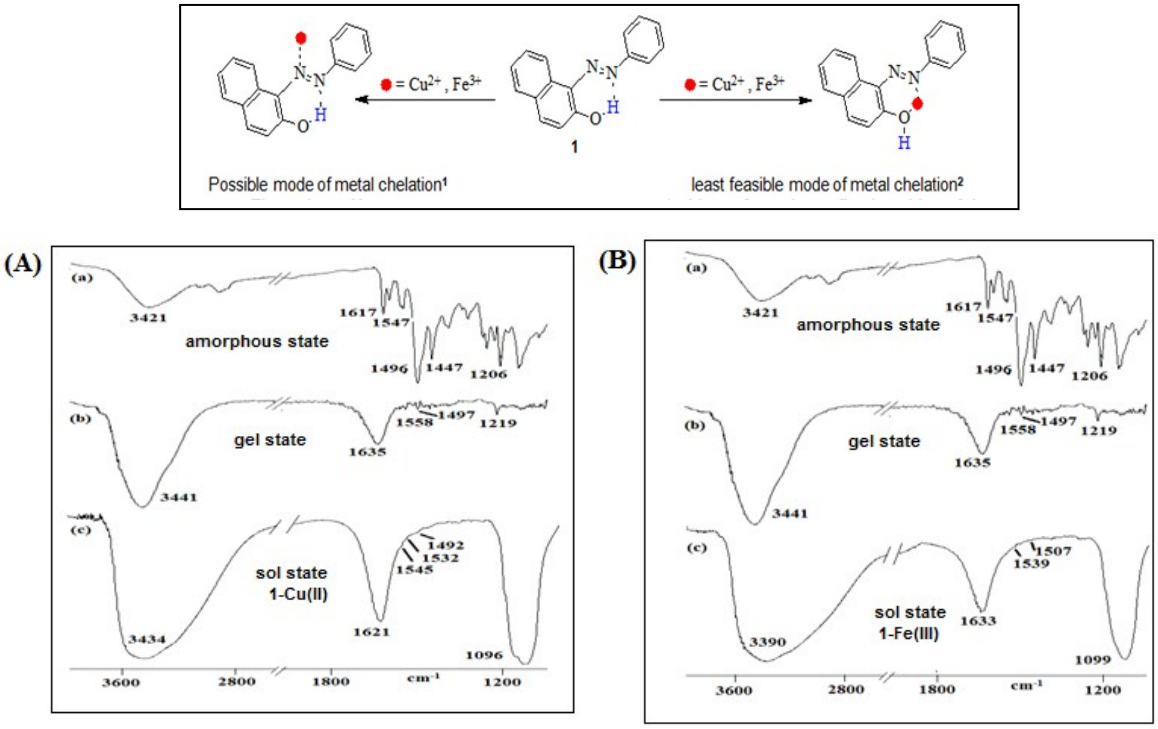

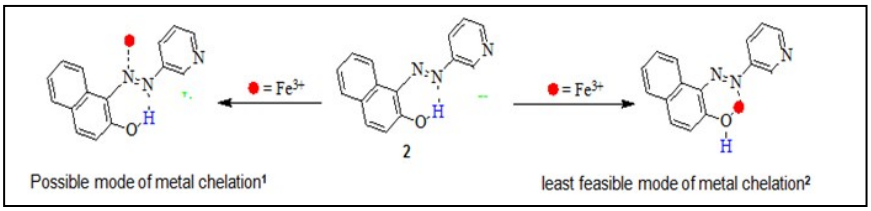

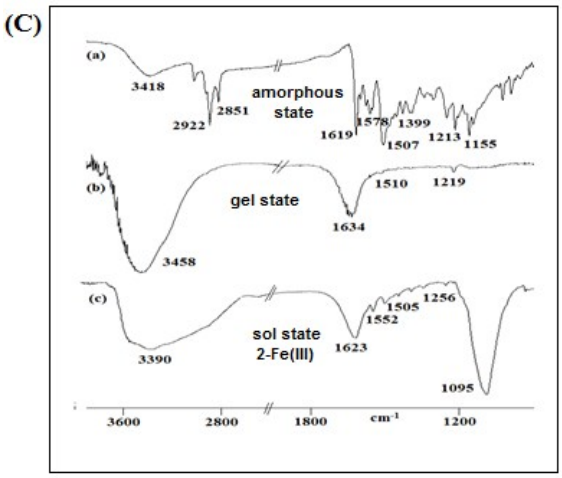

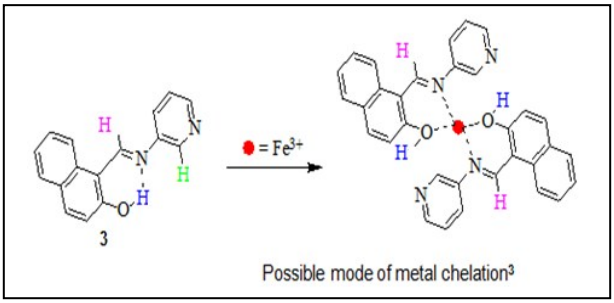

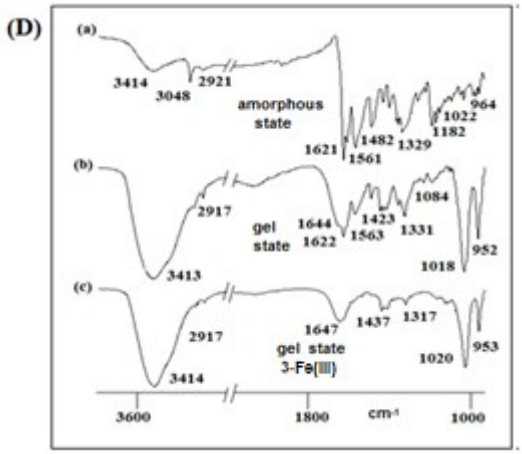

Fig. 14S. Partial FTIR spectra of (A) **1** in (a) amorphous, (b) gel state and (c) sol state with Cu^{2+} ion, (B) **1** in (a) amorphous, (b) gel state and (c) sol state with Fe^{3+} ion, (C) **2** in (a) amorphous, (b) gel state and (c) sol state with Fe^{3+} ion and (D) **3** in (a) amorphous, (b) gel state and (c) gel state with Fe^{3+} ion.

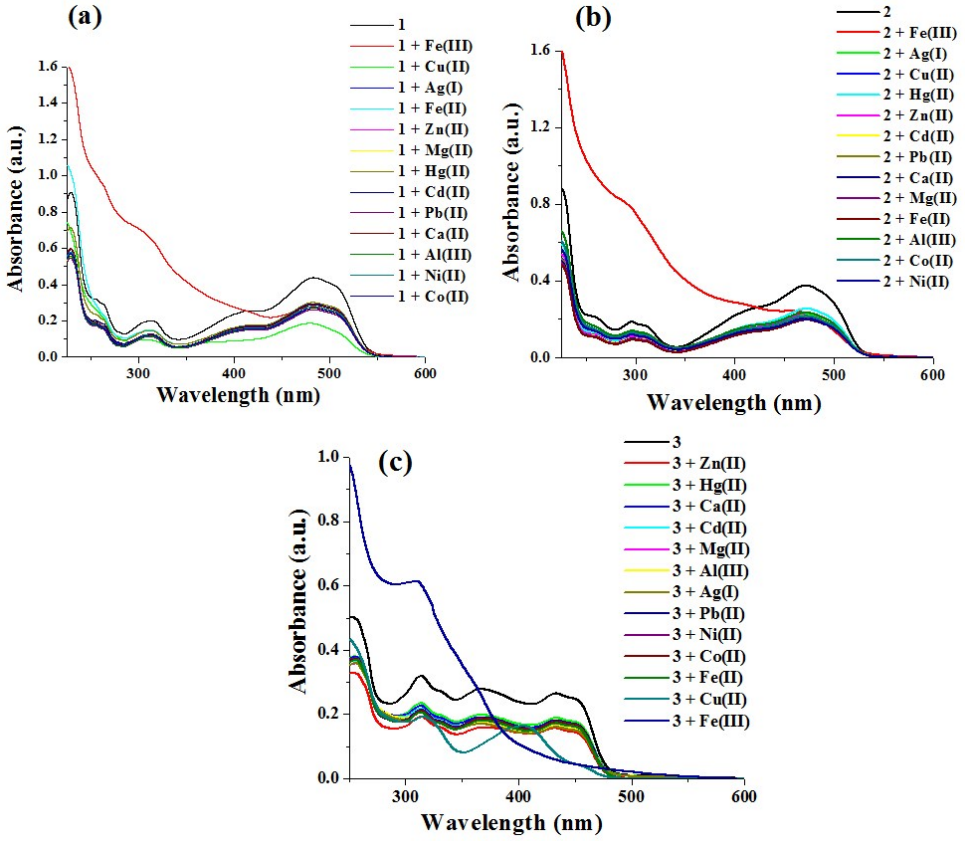

Fig. 15S. Change in absorbance of (a) **1**, (b) **2** and (c) **3** (c = 2.50 x 10^{-5} M) upon addition of 40 equiv. (for **1** and **2**) and 25 equiv. (for **3**) of different metal ions (c = 1.0 x 10^{-3} M) in CH_3CN: H_2O (1:1, v/v).

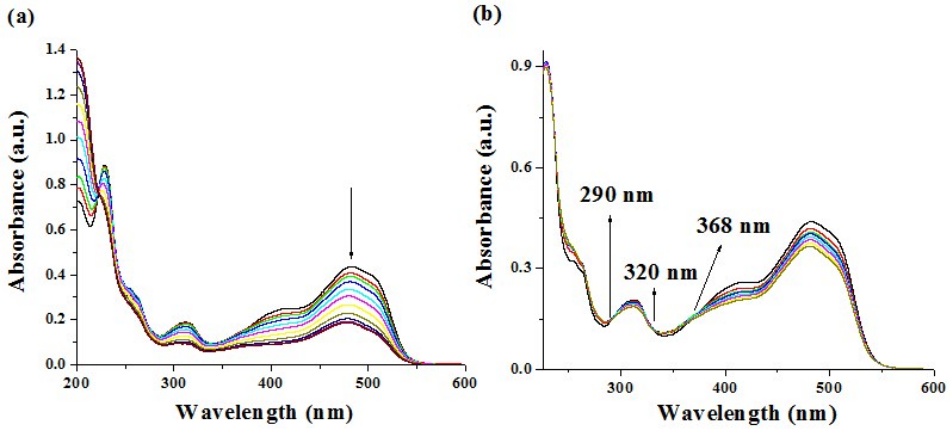

Fig. 16S. Change in absorbance of **1** (c = 2.50 x 10^{-5} M) upon addition of (a) 40 equiv. and (b) 5 equiv. of Cu^{2+} ions (c = 1.0 x 10^{-3} M) in CH_3CN: H_2O (1:1, v/v).

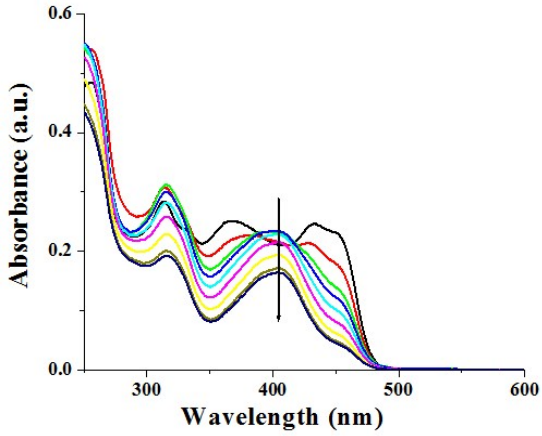

Fig. 17S. Change in absorbance of **3** (c = 2.50 x 10^{-5} M) upon addition of 25 equiv. of Cu^{2+} ions (c = 1.0 x 10^{-3} M) in CH_3CN: H_2O (1:1, v/v).

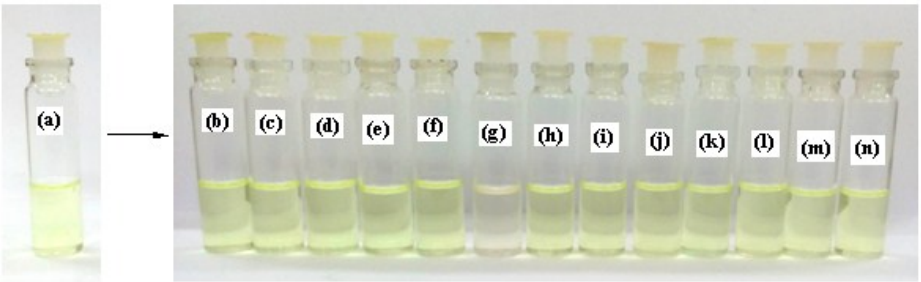

Fig. 18S: Photograph showing the color change of **3** (c = 2.50 x 10^{-5} M) in presence of 25 equiv. of different metal ions (a) **3**, (b) Cu^{2+}, (c) Hg^{2+}, (d) Zn^{2+}, (e) Cd^{2+}, (f) Al^{3+} (g) Fe^{3+}, (h) Fe^{2+}, (i) Ag^{+}, (j) Pb^{2+}, (k) Co^{2+}, (l) Ni^{2+}, (m) Mg^{2+} and (n) Ca^{2+} (c = 1.0 x 10^{-3} M) in CH_3CN: H_2O (1:1, v/v).

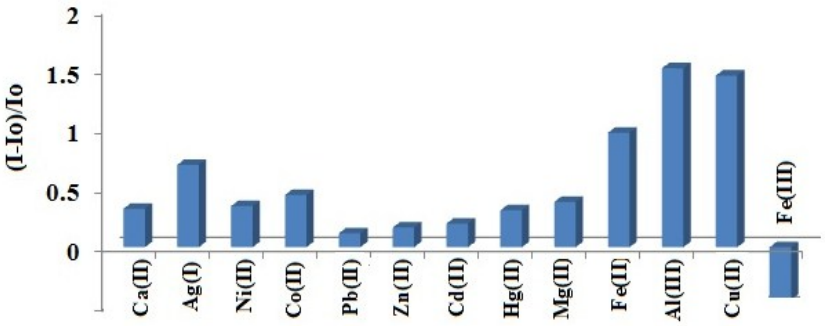

Fig. 19S. Change in fluorescence ratio (λ_{ex} = 310 nm) of **1** (c = 2.5 x 10^{-5} M) at 412 nm upon addition of 40 equiv. amounts of ions (c = 1.0 x 10^{-3} M) in CH_3CN: H_2O (1:1, v/v).

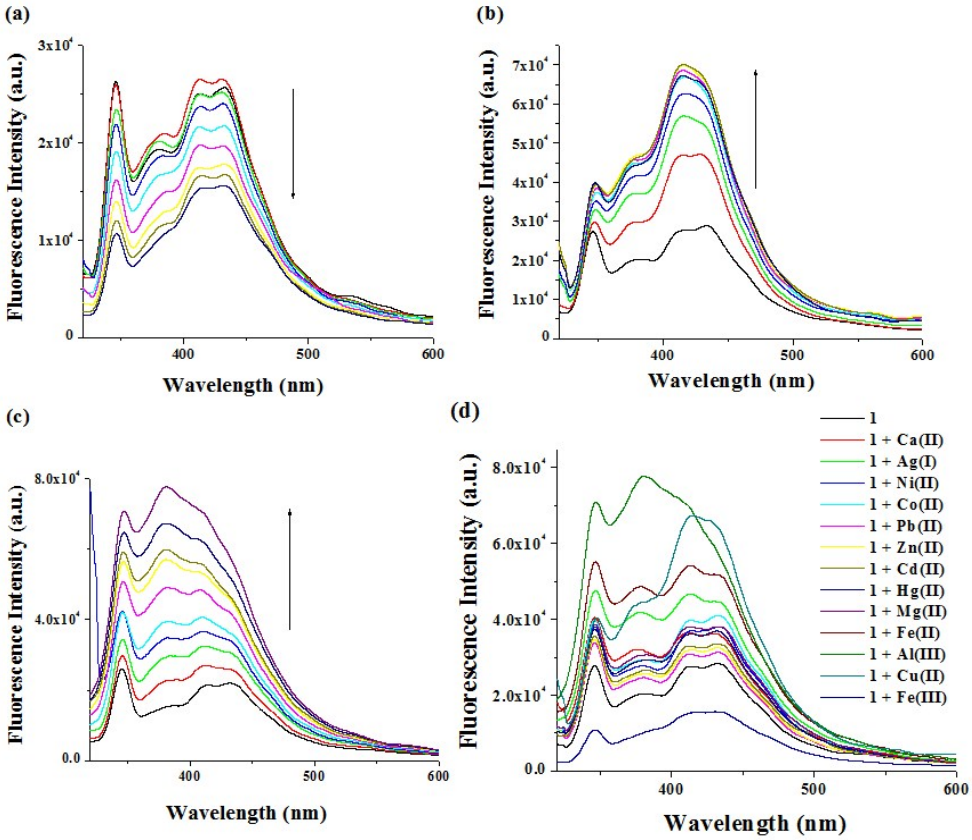

Fig. 20S. Change in fluorescence intensity of **1** (c = 2.50 x 10^{-5} M) upon addition of 40 equiv. of (a) Fe^{3+}, (b) Cu^{2+}, (c) Al^{3+} and (d) all metal ions (c = 1.0 x 10^{-3} M) in CH_3CN: H_2O (1:1, v/v).

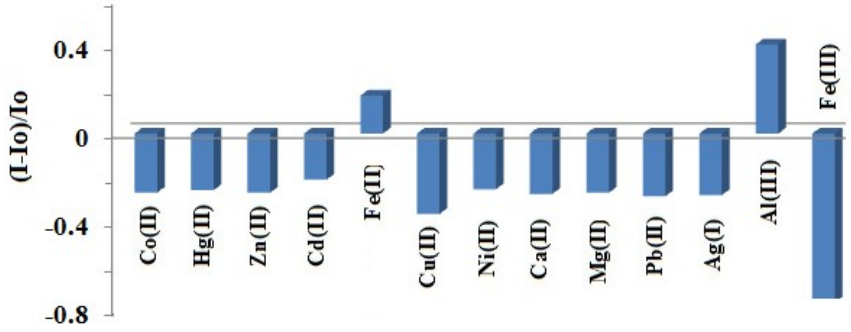

Fig. 21S. Change in fluorescence ratio (λ_{ex} = 310 nm) of **2** (c = 2.5 x 10^{-5} M) at 346 nm upon addition of 40 equiv. amounts of ions (c = 1.0 x 10^{-3} M) in CH_3CN: H_2O (1:1, v/v).

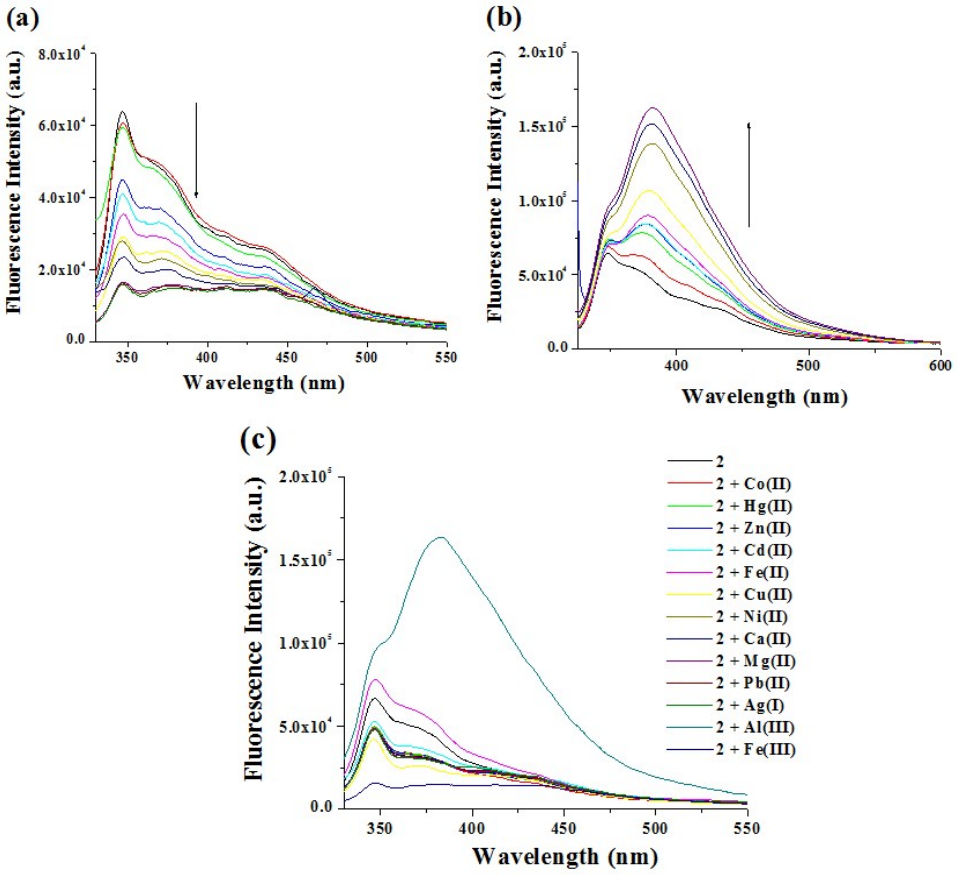

Fig. 22S. Change in fluorescence intensity of **2** (c = 2.50 x 10^{-5} M) upon addition of 40 equiv. of (a) Fe^{3+}, (b) $Al^{3+}$and (c) all metal ions (c = 1.0 x 10^{-3} M) in CH_3CN: H_2O (1:1, v/v).

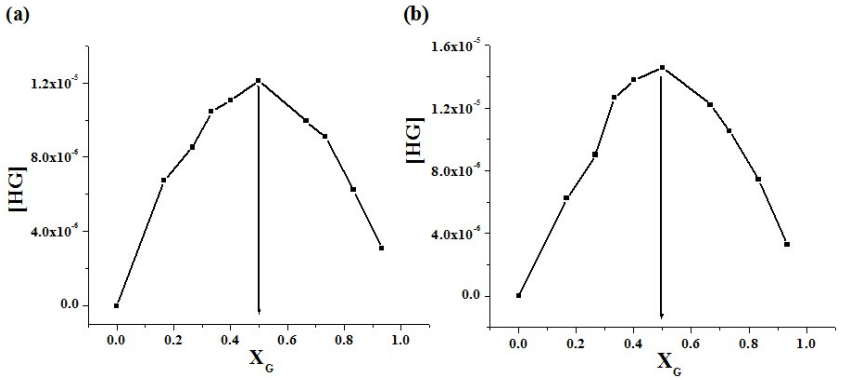

Fig. 23S. Job plot of receptor **1** (c = 2.5 x 10^{-5} M) with (a) Fe^{3+} and (b) Cu^{2+} from UV.

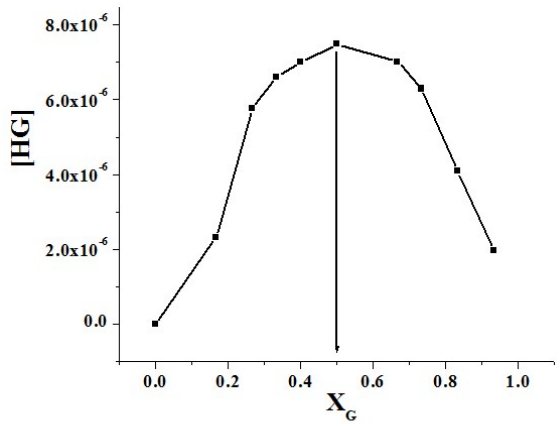

Fig. 24S. Job plot of receptor **2** (c = 2.5 x 10^{-5} M) with Fe^{3+} from UV.

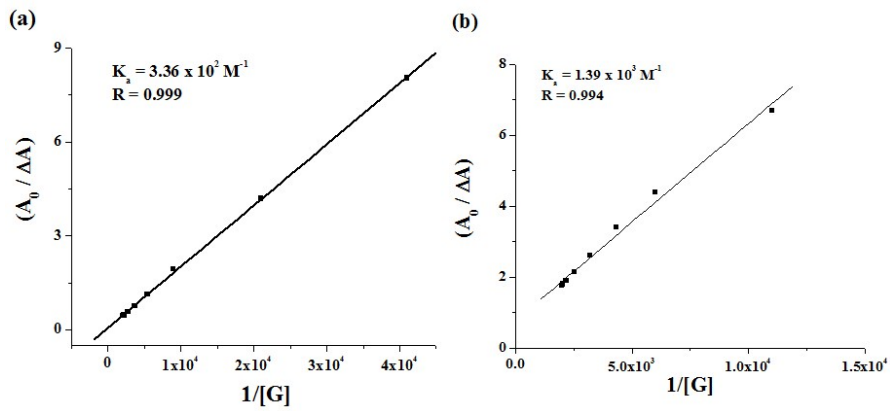

Fig. 25S. Benesi–Hilderband plot for **1** (c = 2.5 x 10^{-5} M) with (a) Fe^{3+} at 312 nm and (b) Cu^{2+} at 480 nm (c = 1.0 x 10^{-3} M) in CH_3CN: H_2O (1:1, v/v) from UV.

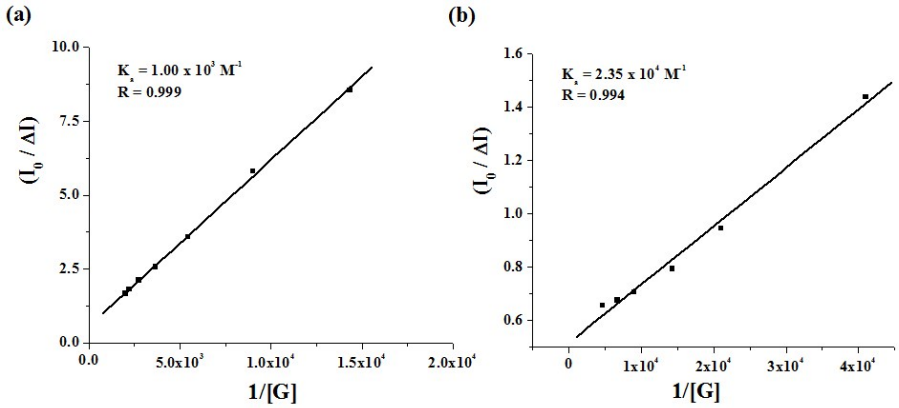

Fig. 26S. Benesi–Hilderband plot for **1** (c = 2.5 x 10^{-5} M) with (a) Fe^{3+} at 345 nm and (b) Cu^{2+} at 414 nm (c = 1.0 x 10^{-3} M) in CH_3CN: H_2O (1:1, v/v) from fluorescence.

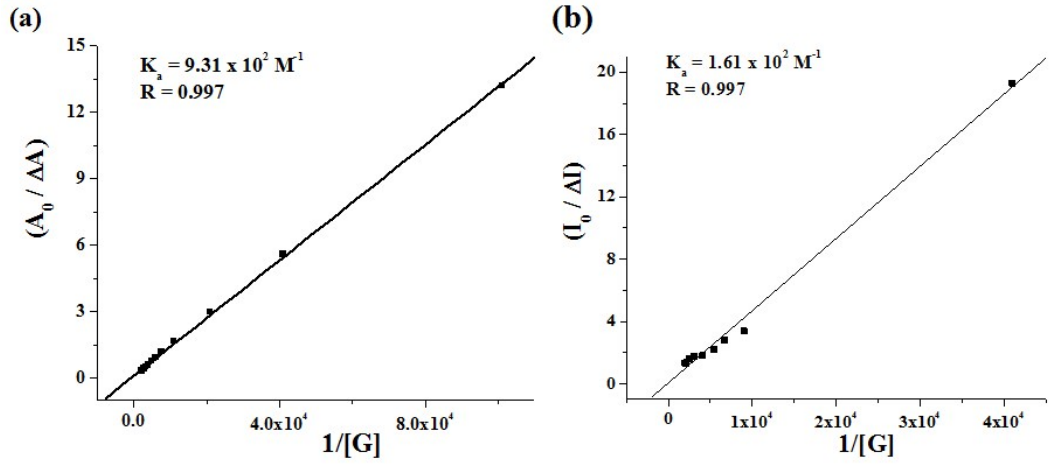

Fig. 27S. Benesi–Hilderband plot for **2** (c = 2.5 x 10^{-5} M) with Fe^{3+} from (a) UV at 295 nm and (b) fluorescence at 346 nm (c = 1.0 x 10^{-3} M) in CH_3CN: H_2O (1:1, v/v).

HRMS spectra of the metal-ligand complexes of 1 and 2

(a)

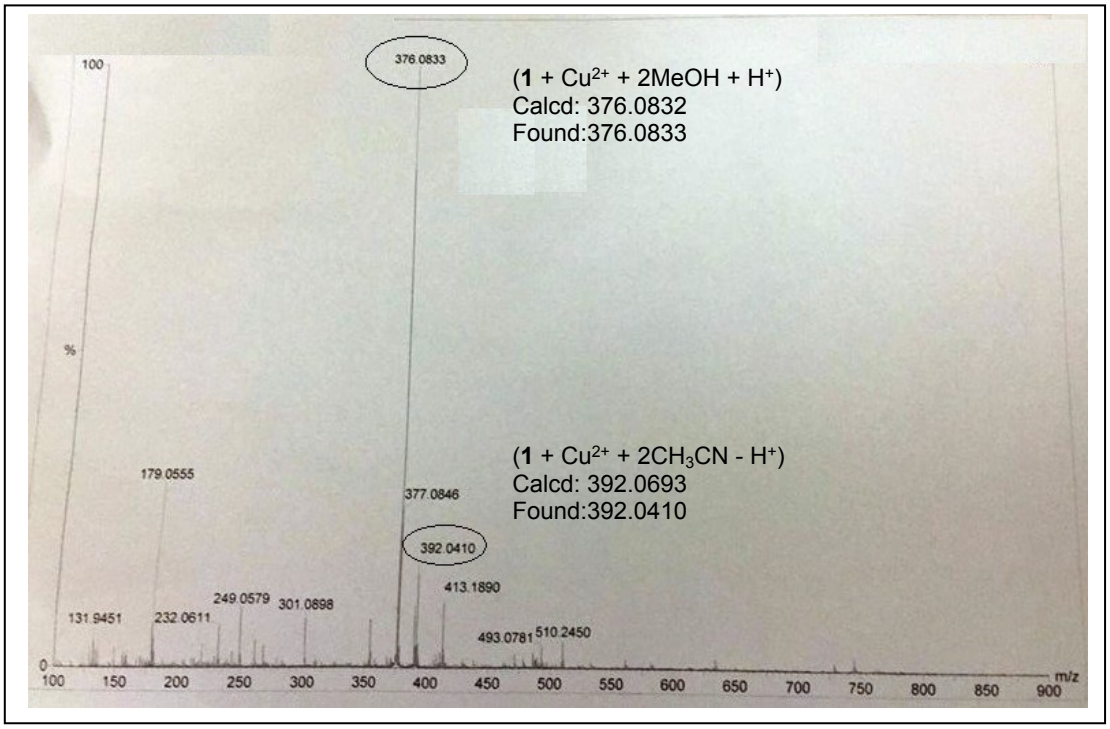

(b)

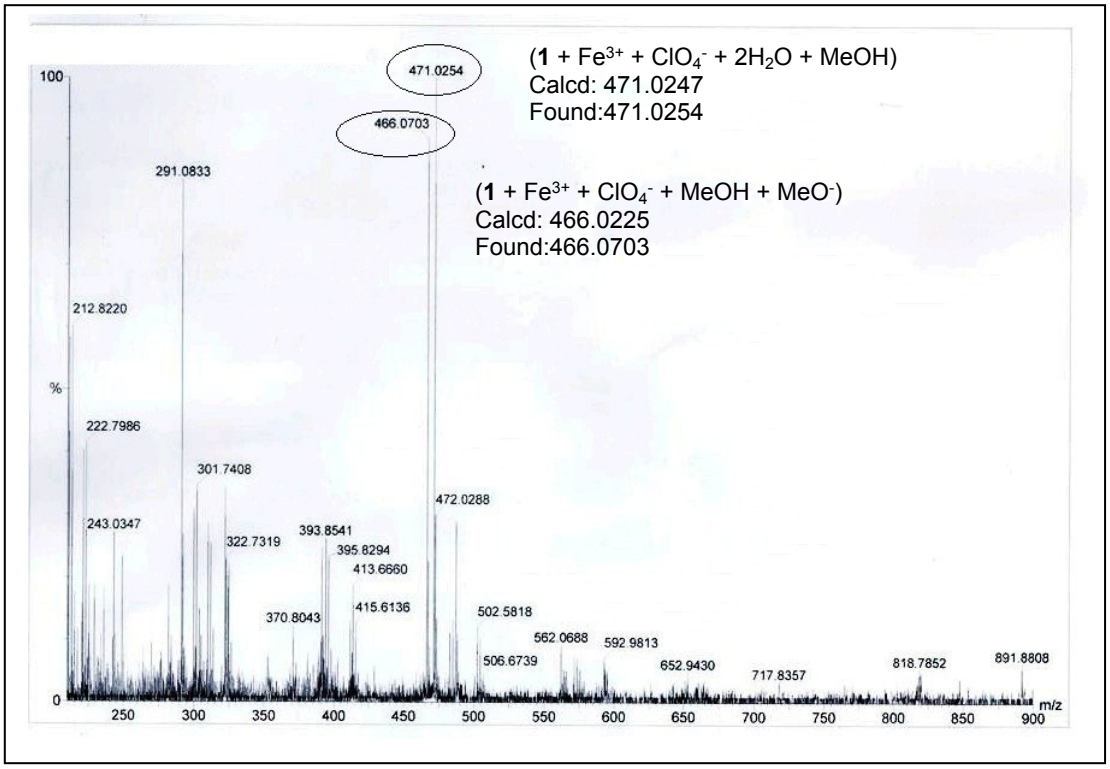

(c)

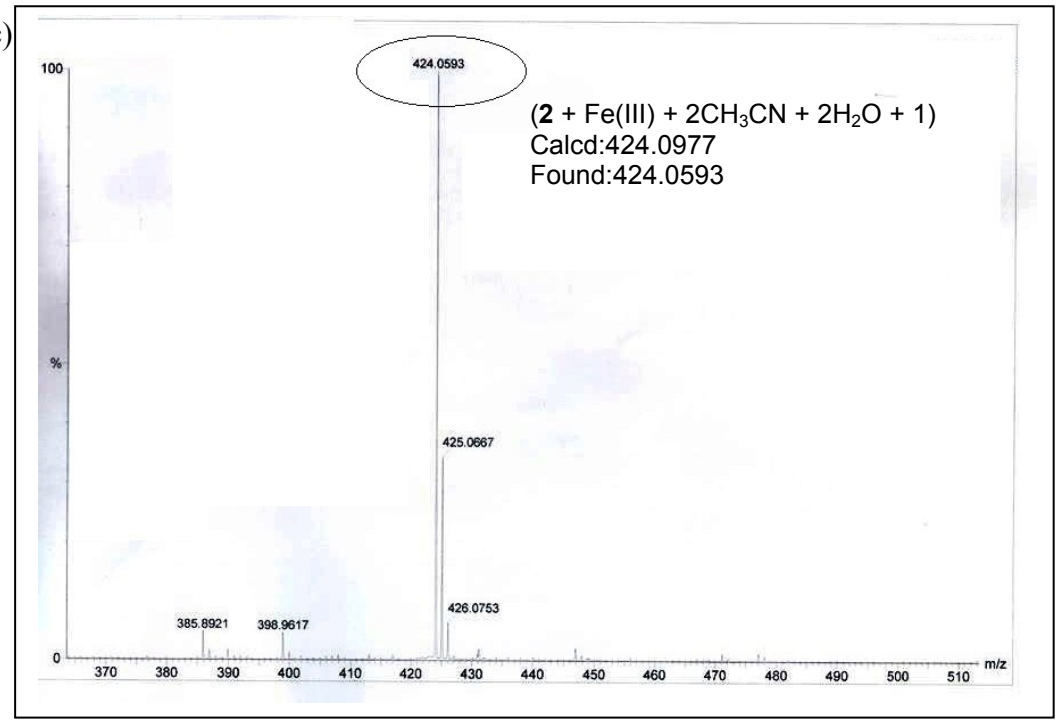

Fig. 28S. HRMS spectra of (a) **1**-Cu^{2+}, (b) **1**-Fe^{3+} and (c) **2**-Fe^{3+} complexes.

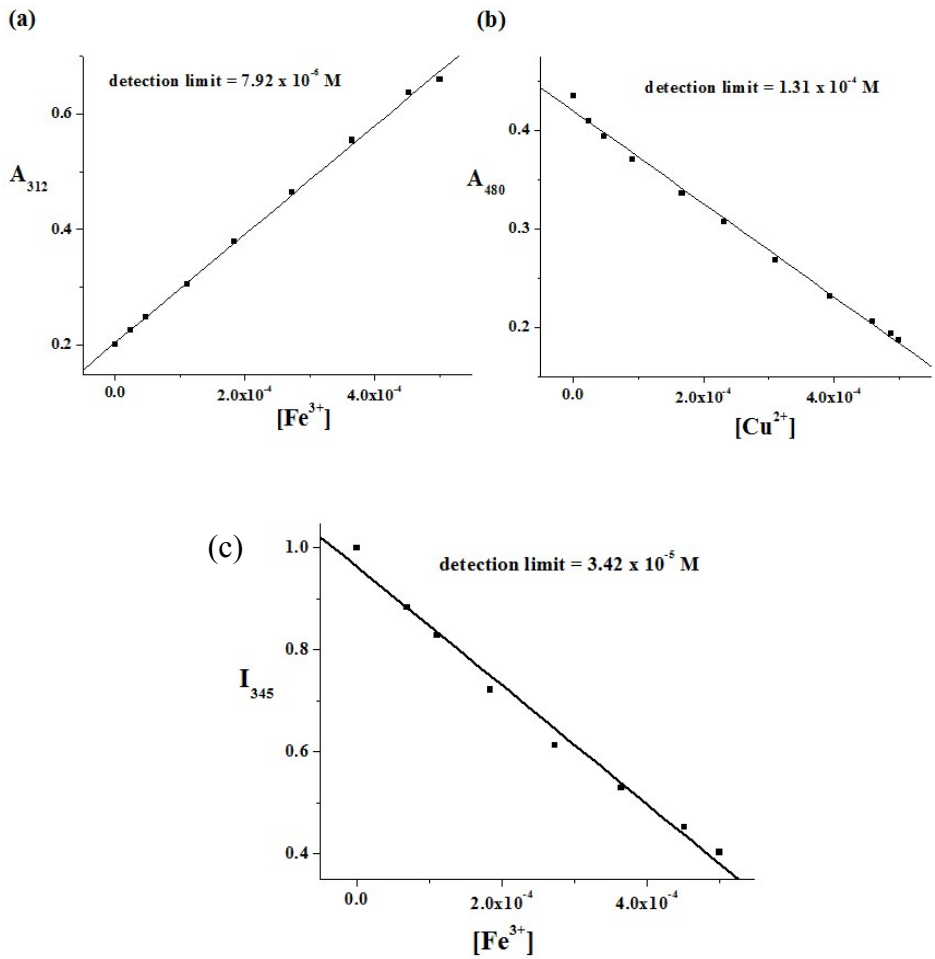

Fig. 29S. Detection limit of (a) Fe^{3+} and (b) Cu^{2+} in CH_3CN: H_2O (1:1, v/v) from UV-vis titration and (c) detection limit of Fe^{3+} in CH_3CN: H_2O (1:1, v/v) from fluorescence for compound **1**.

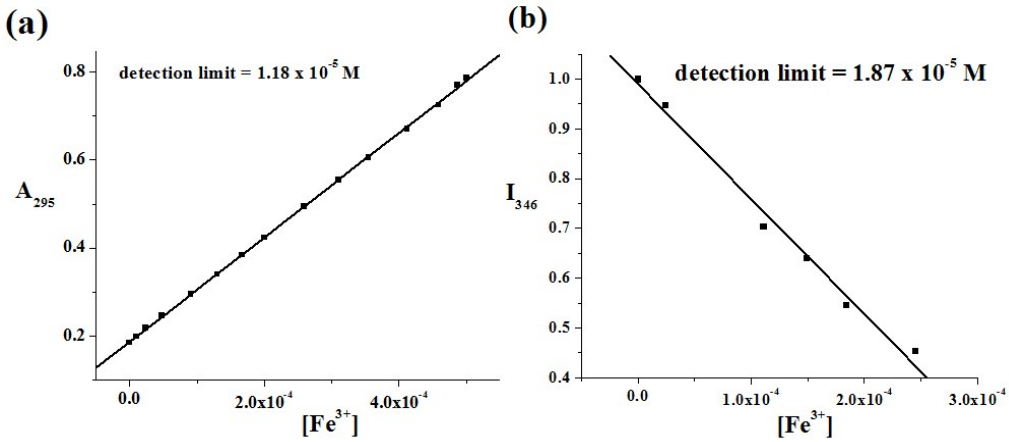

Fig. 30S. Detection limit of Fe^{3+} from (a) UV and (b) fluorescence in CH_3CN: H_2O (1:1, v/v) for compound **2**.

Table 2S. Binding constants and detection limit values for the metal ligand complexes.

Metal ligand complex	Binding constant values (M^{-1})	
	From UV-vis titration	From fluorescence titration
1 – Fe^{3+}	K = 3.36 x 10^2	K = 1.00 x 10^3
1 - Cu^{2+}	K = 1.39 x 10^3	K = 2.35 x 10^4
2 – Fe^{3+}	K = 9.31 x 10^2	K = 1.61 x 10^2
3 – Fe^{3+}	K_1 = (6.48 ± 1.24) x 10^4 K_2 = (5.34 ± 0.67) x 10^2	K_1 = (6.68 ± 1.44) x 10^4 K_2 = (1.05 ± 0.36) x 10^4

Metal ligand complex	Detection limit values (M)	
	From UV-vis titration	From fluorescence titration
1 – Fe^{3+}	7.92 x 10^{-6}	1.31 x 10^{-4}
1 – Cu^{2+}	3.42 x 10^{-5}	-
2 – Fe^{3+}	1.18 x 10^{-6}	1.87 x 10^{-5}
3 – Fe^{3+}	6.67 x 10^{-6}	9.76 x 10^{-7}

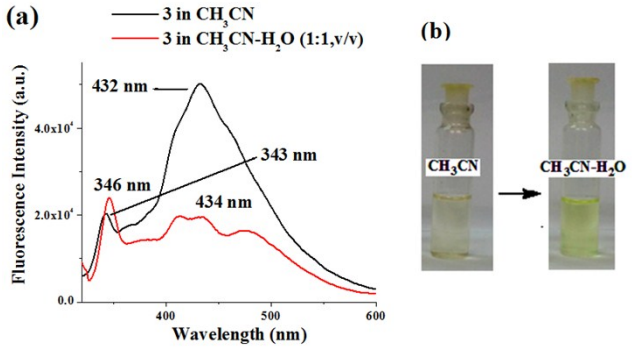

Fig. 31S. (a) Fluorescence spectra of **3** (c = 2.50 x 10^{-5} M) in CH_3CN and CH_3CN: H_2O (1:1, v/v) and (b) the respective color of the solutions.

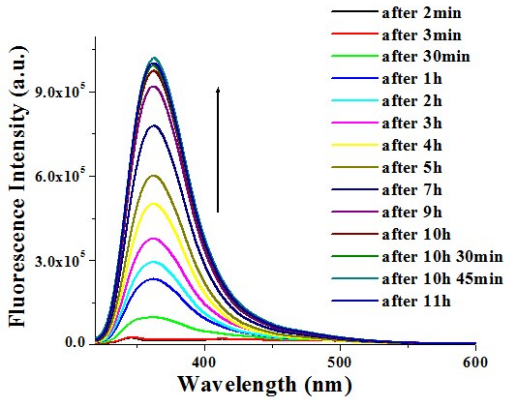

Fig. 32S. Change in fluorescence intensity of **3** (c = 2.50 x 10^{-5} M) with time in CH_3CN: H_2O (1:1, v/v).

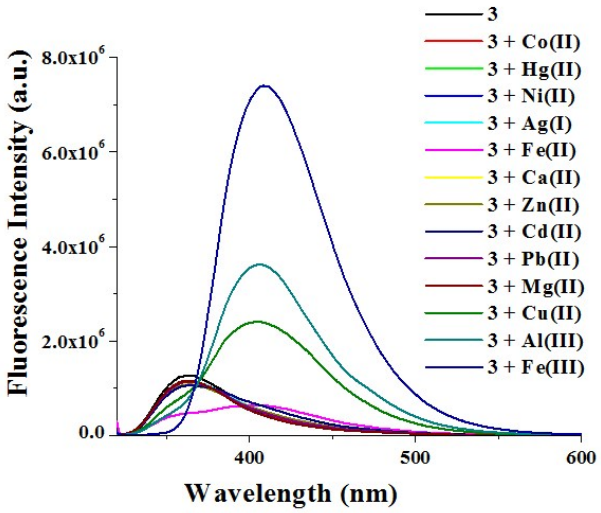

Fig. 33S. Change in fluorescence intensity of **3** (c = 2.50 x 10^{-5} M) upon addition of 10 equiv. (a) Fe^{2+}, (b) Al^{3+}, (b) Cu^{2+} and (c) different metal ions (c = 1.0 x 10^{-3} M) in CH_3CN: H_2O (1:1, v/v).

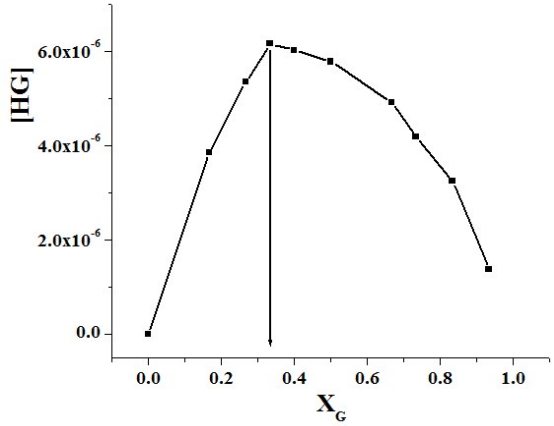

Fig. 34S. Job plot of receptor **3** (c = 2.5 x 10^{-5} M) with Fe^{3+} UV.

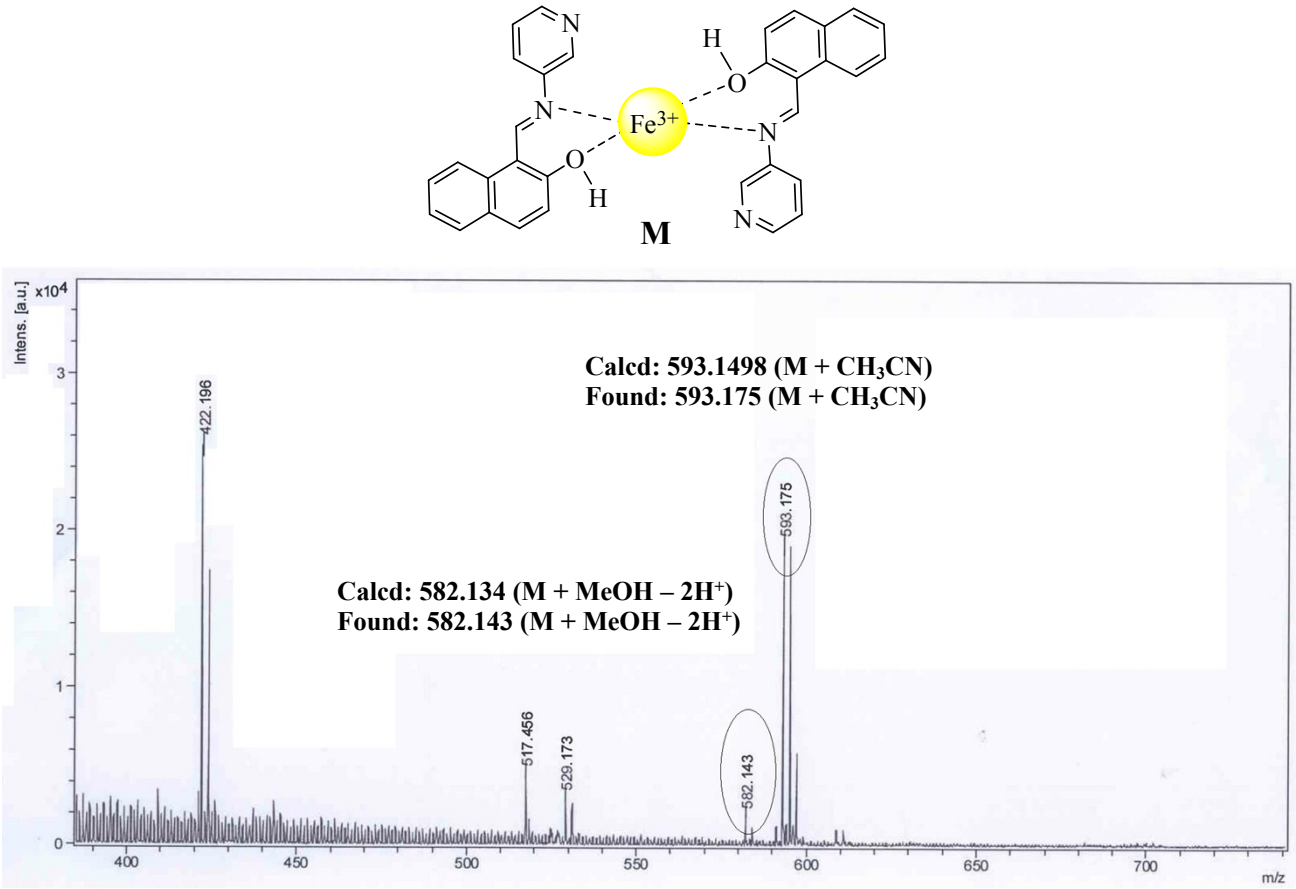

Fig. 35S. Mass spectrum of the **3**-Fe (III) complex and suggested binding mode.

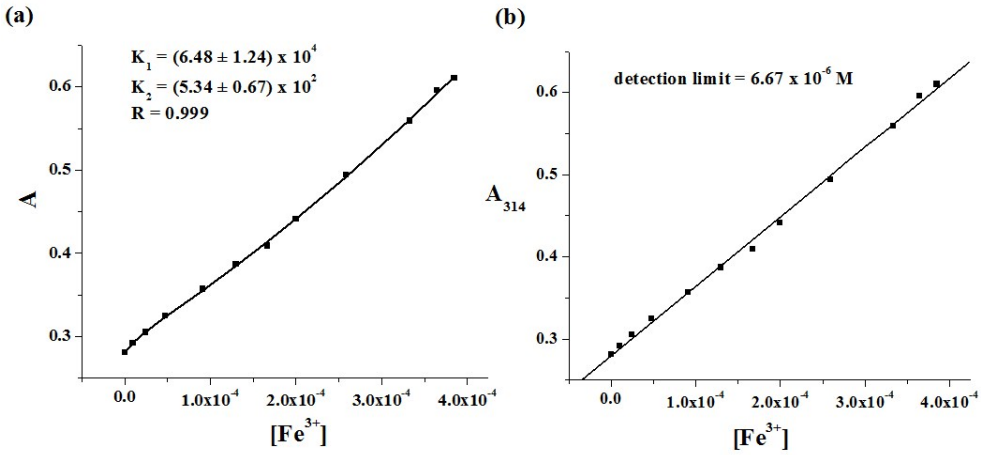

Fig. 36S. (a) Non liner binding constant curve for receptor **3** (c = 2.5 x 10^{-5} M) and (b) Detection limit of Fe^{3+} from UV.

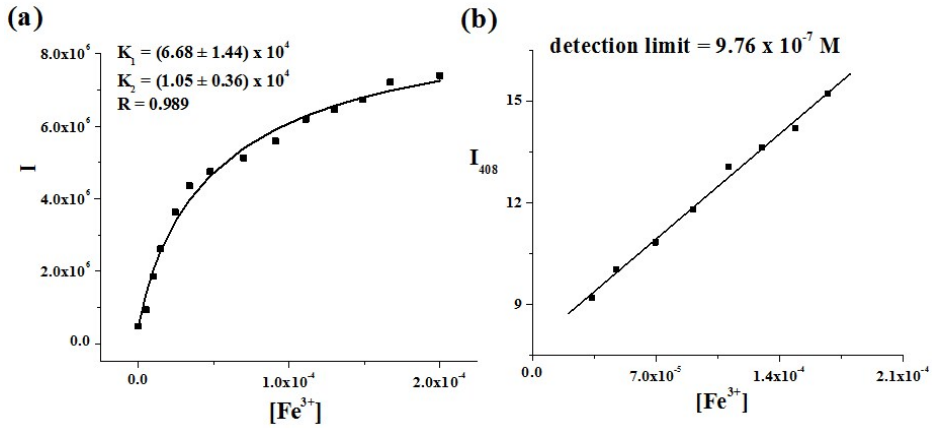

Fig. 37S. (a) Non liner binding constant curve for receptor **3** (c = 2.5 x 10^{-5} M) and (b) Detection limit of Fe^{3+} from fluorescence.

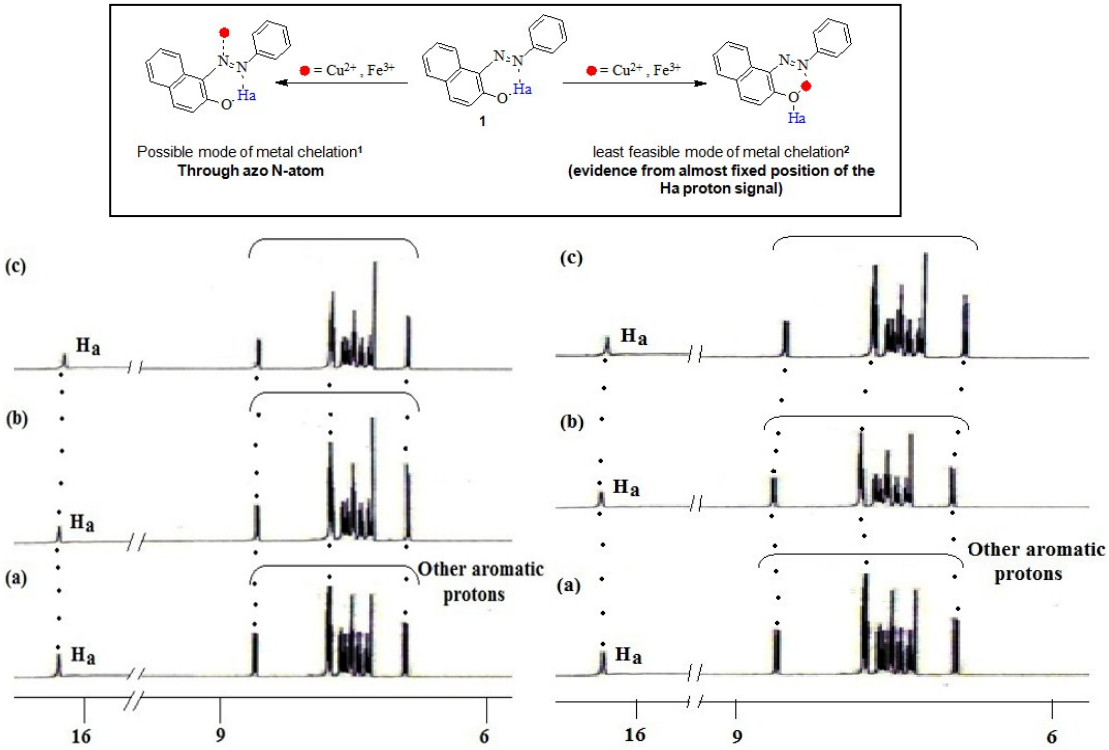

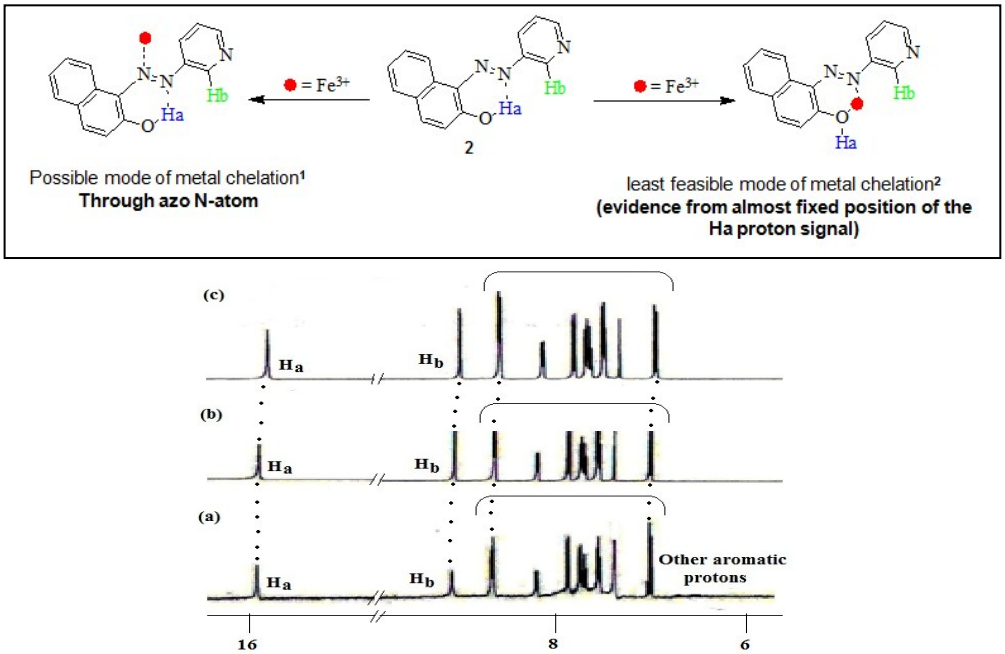

Fig. 38S. ^{1}H NMR titration of (a) **1** (c = 0.012 M) with (b) 0.5 equiv. and (c) 1 equiv. of Cu^{2+} (c = 0.067 M) (left) and Fe^{3+} (c = 0.636 M) (right) in $CDCl_3$ (top). ^{1}H NMR titration of (a) **2** (c = 0.037 M) with (b) 0.5 equiv. and (c) 1 equiv. of Fe^{3+} (c = 0.636 M) in $CDCl_3$ (bottom).

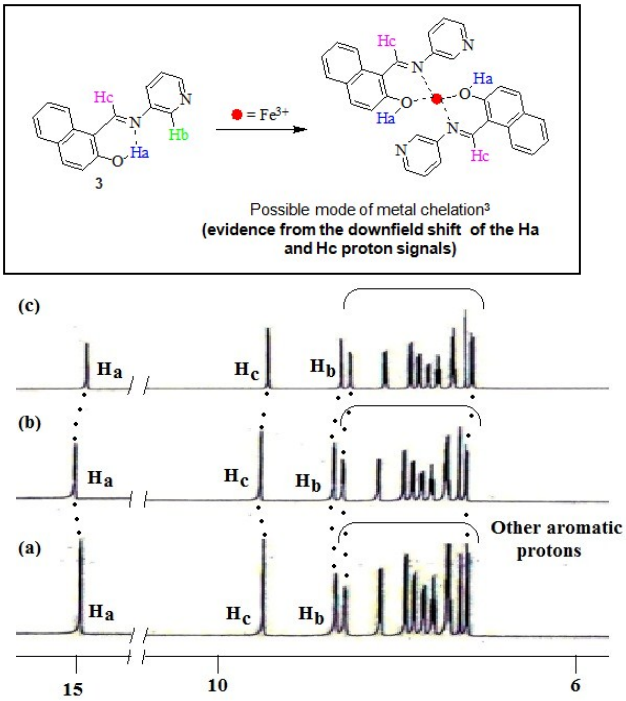

Fig. 39S. ^{1}H NMR titration of (a) **3** (c = 0.02 M) with (b) 0.5 equiv. and (c) 1 equiv. of Fe^{3+} (c = 0.636 M) in $CDCl_3$.

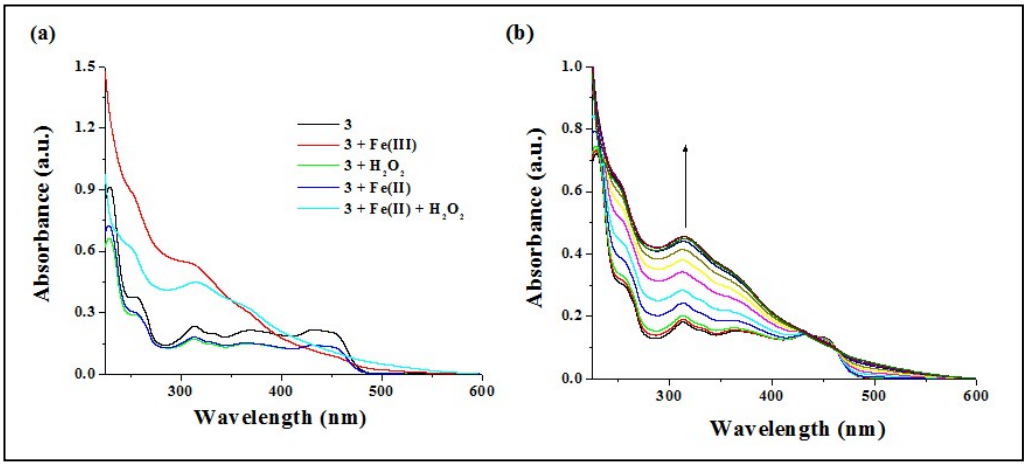

Fig. 40S. Absorption spectra of (a) **3** (c = 2.50 x 10^{-5} M) in presence of Fe^{3+}, Fe^{2+}, H_2O_2 (25 equiv.) and mixture of Fe^{2+} and H_2O_2 (c = 1.0 x 10^{-3} M) and (b) **3** (c = 2.50 x 10^{-5} M) + 25 equiv. of Fe^{2+} (c = 1.0 x 10^{-3} M) in presence of 15 equiv. of H_2O_2 (c = 1.0 x 10^{-3} M) in CH_3CN: H_2O (1:1, v/v).

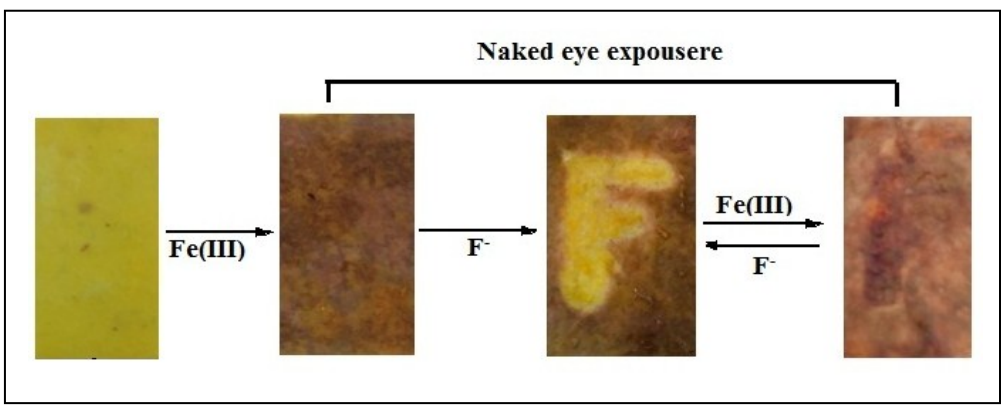

Fig. 41S. Pictorial representation of **3**-Fe(III) system as rewritable display material (for **3**, c = 0.001 M and for Fe^{3+} and F^-, c = 0.05 M)

^{1}H NMR ($CDCl_3$, 400 MHz)

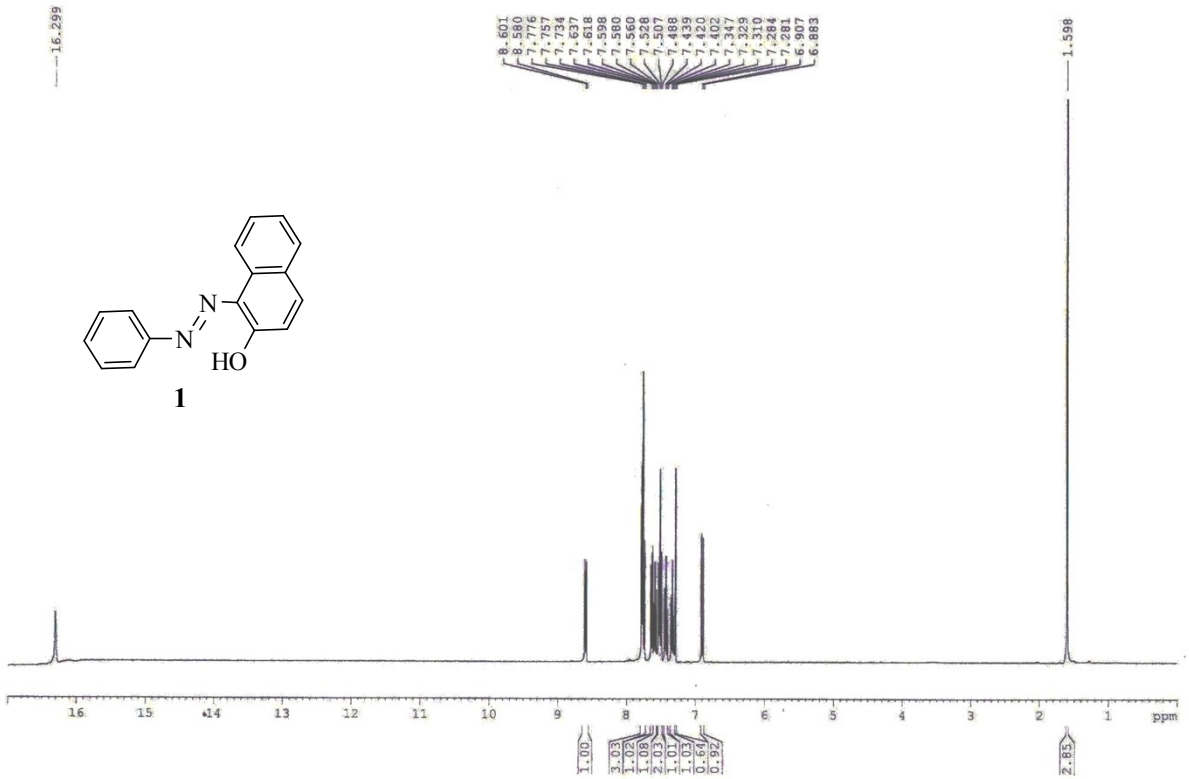

^{13}C NMR ($CDCl_3$, 100 MHz)

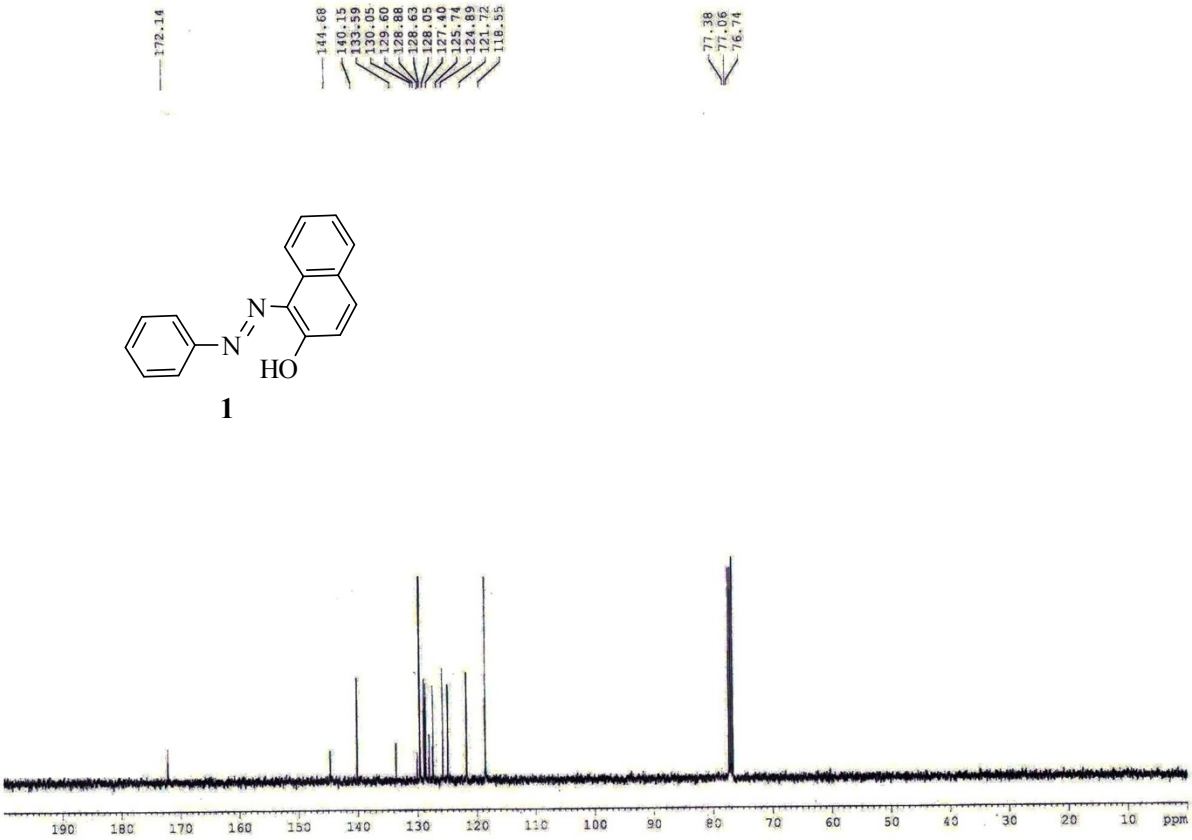

Mass spectrum of 1.

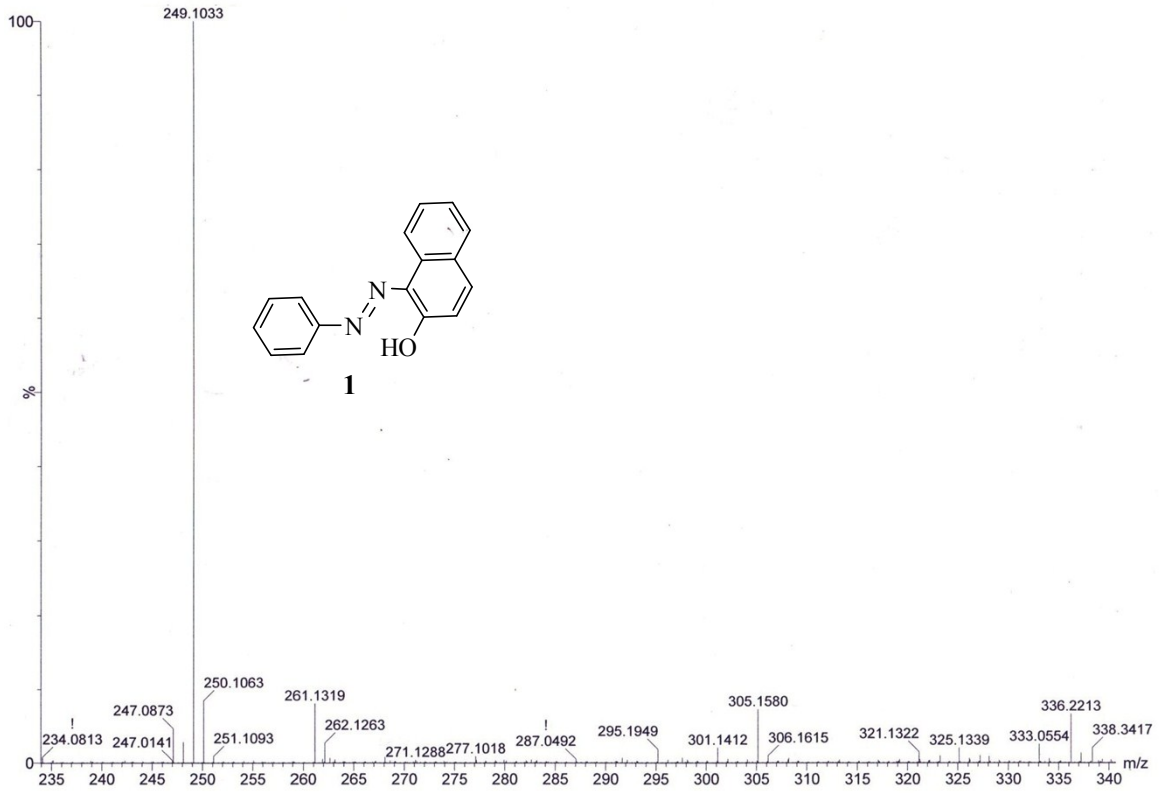

^{1}H NMR ($CDCl_3$, 400 MHz)

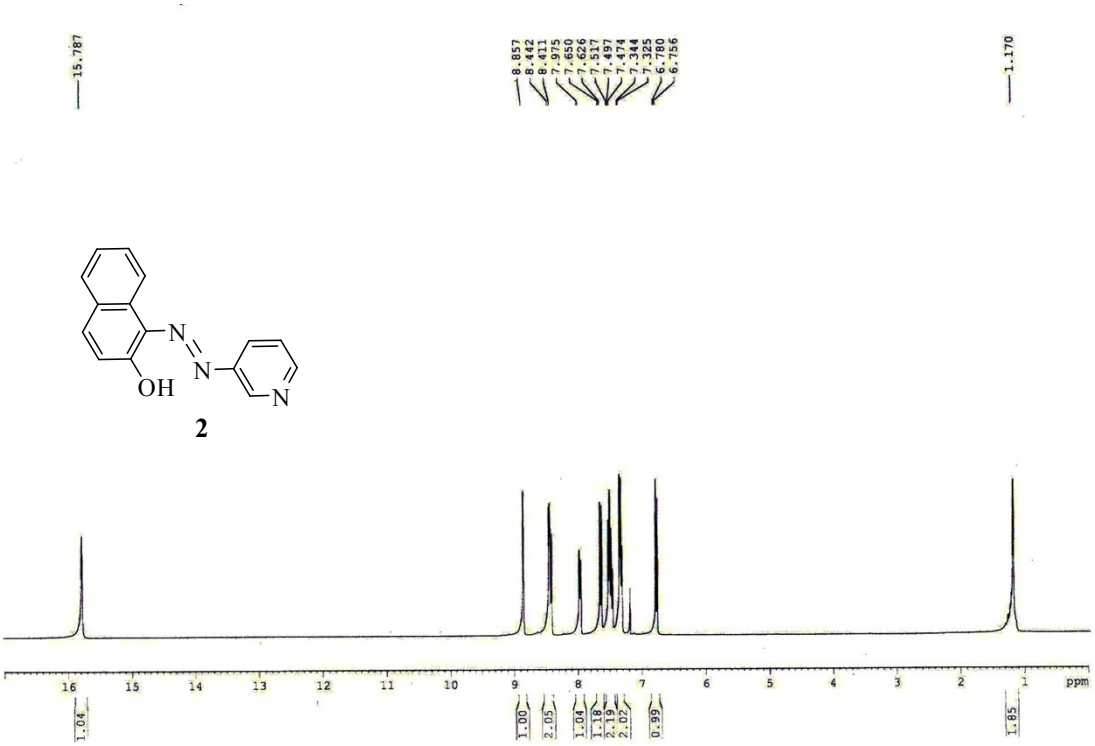

^{13}C NMR ($CDCl_3$, 100 MHz)

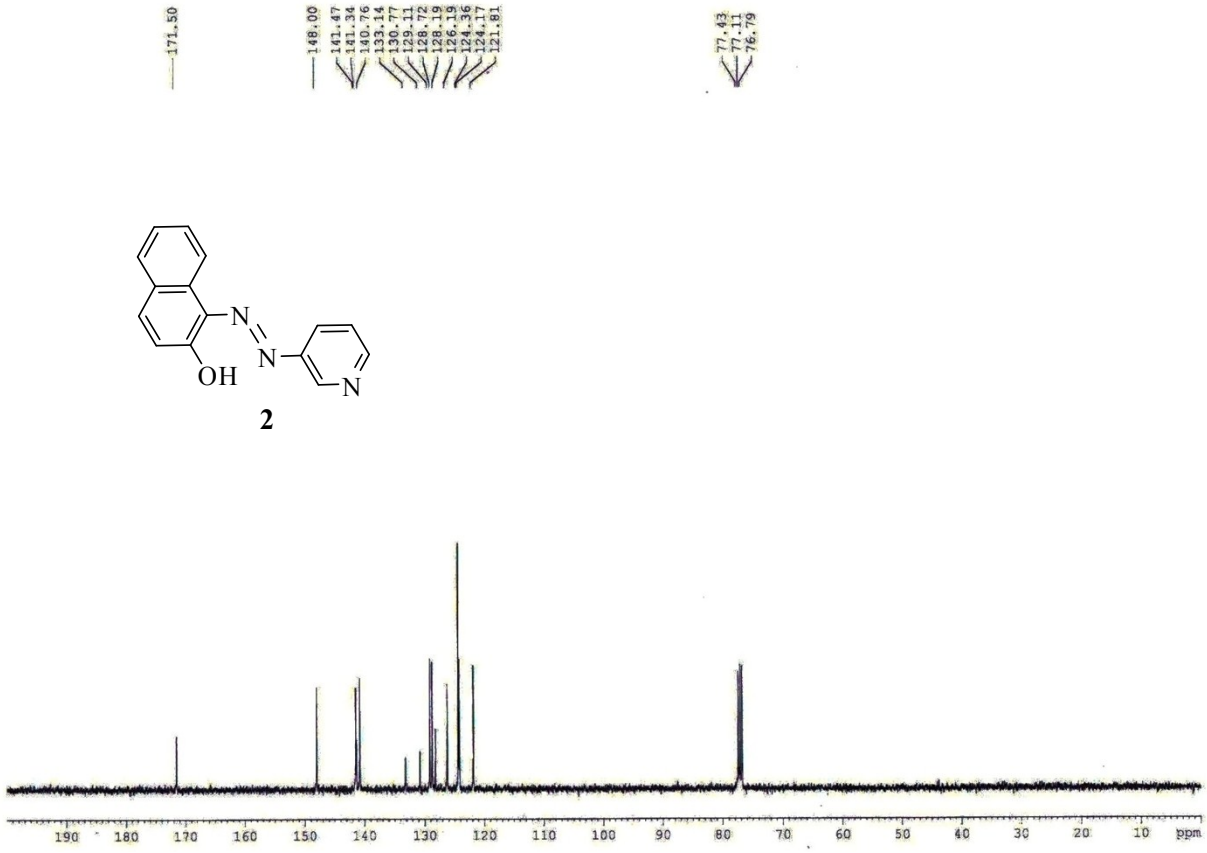

2

Mass spectrum of 2.

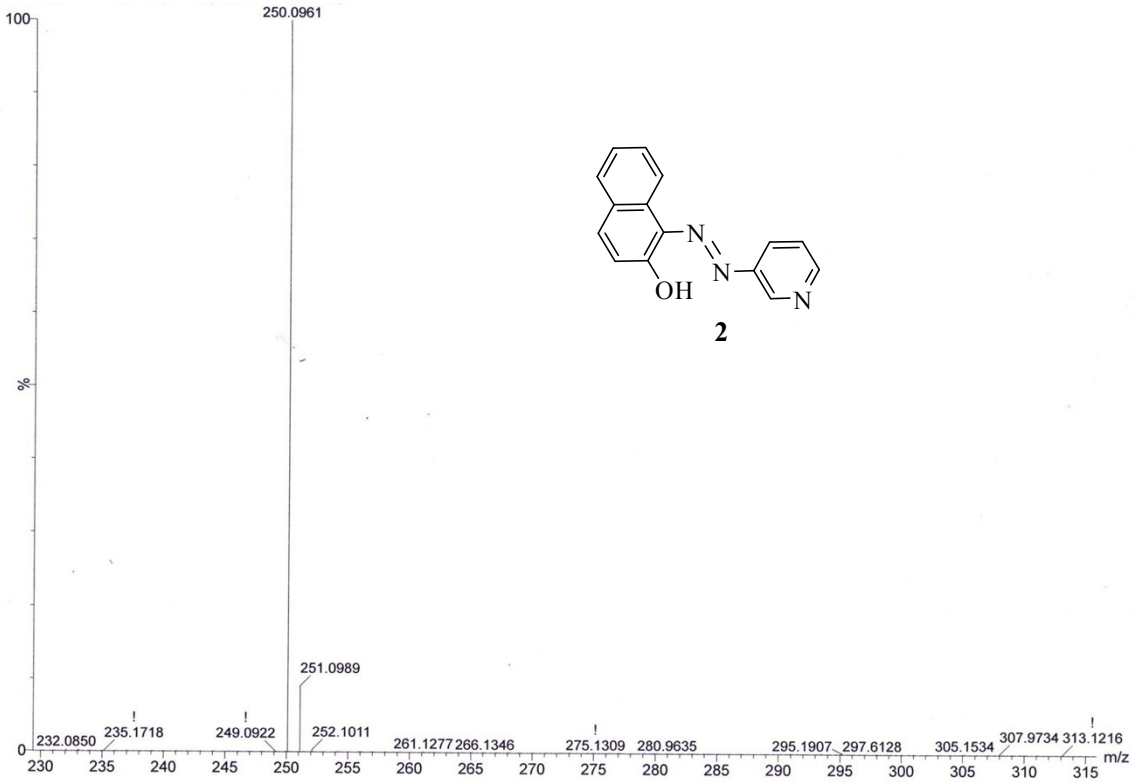

^{1}H NMR ($CDCl_3$, 400 MHz)

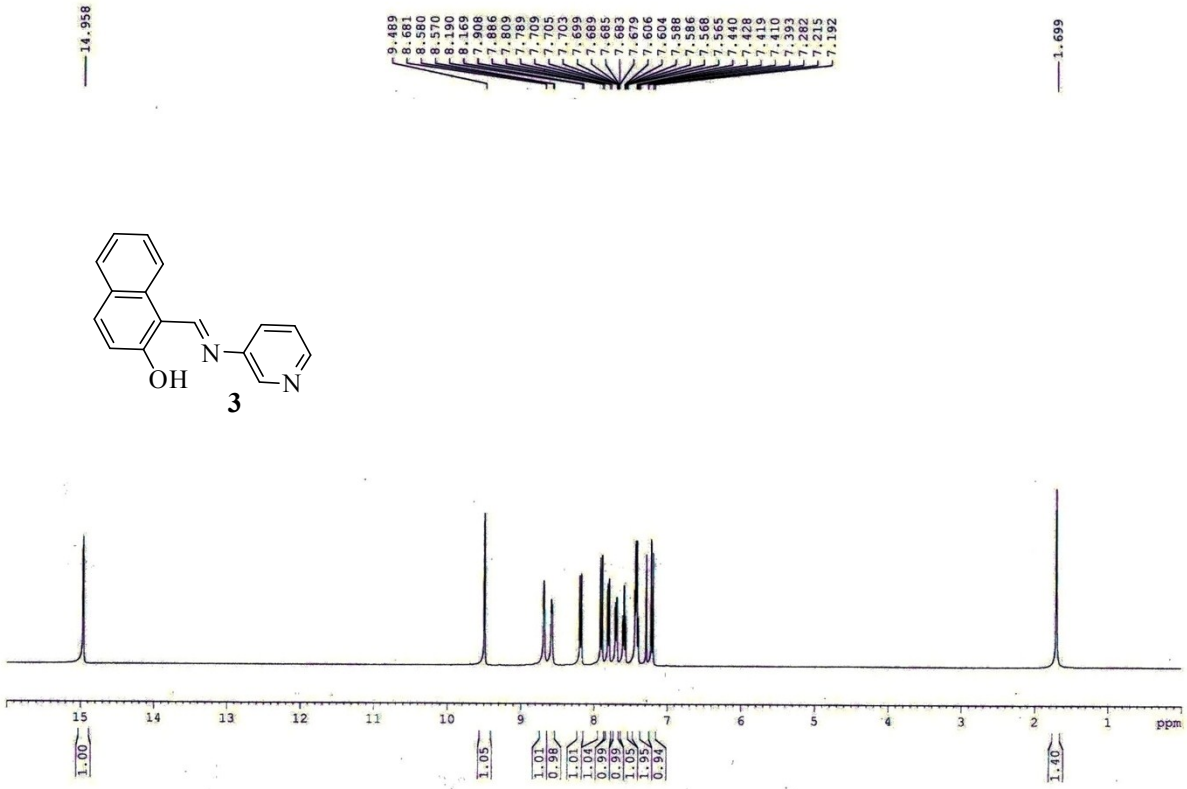

^{13}C NMR ($CDCl_3$, 100 MHz)

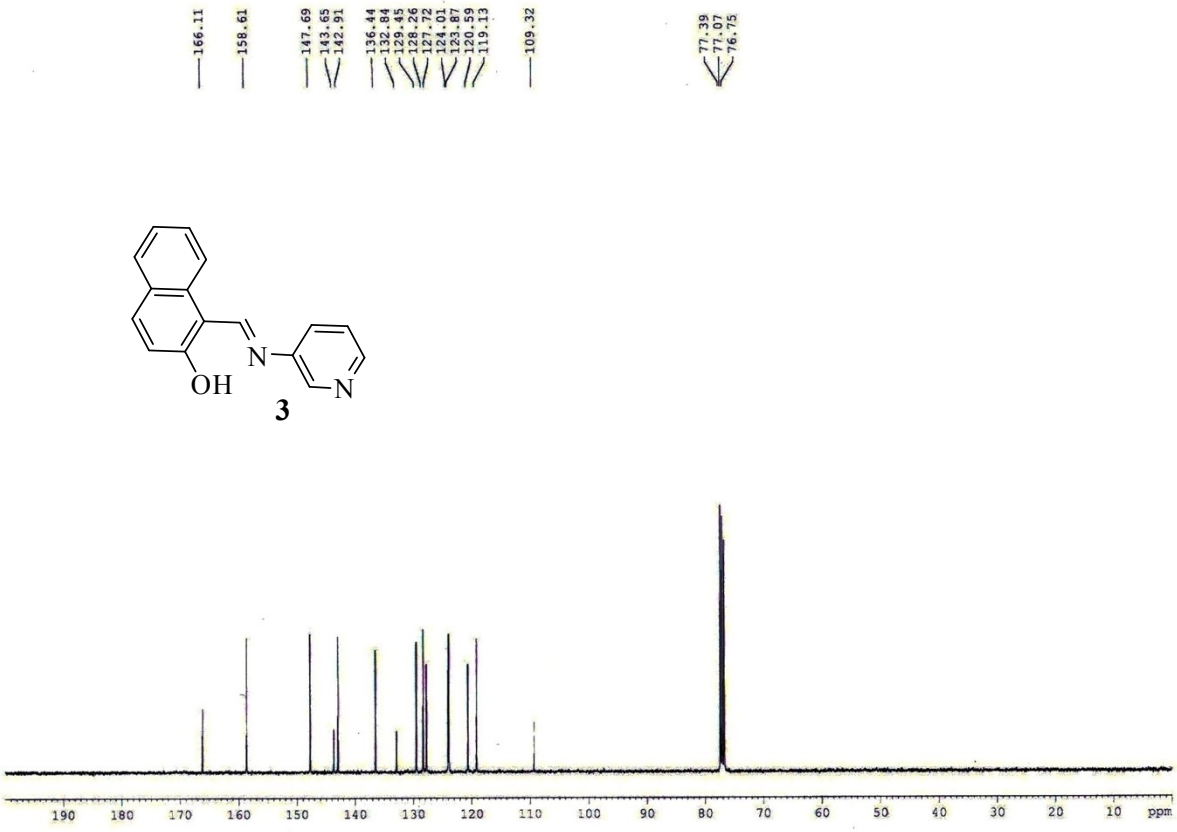

Mass spectrum of 3.

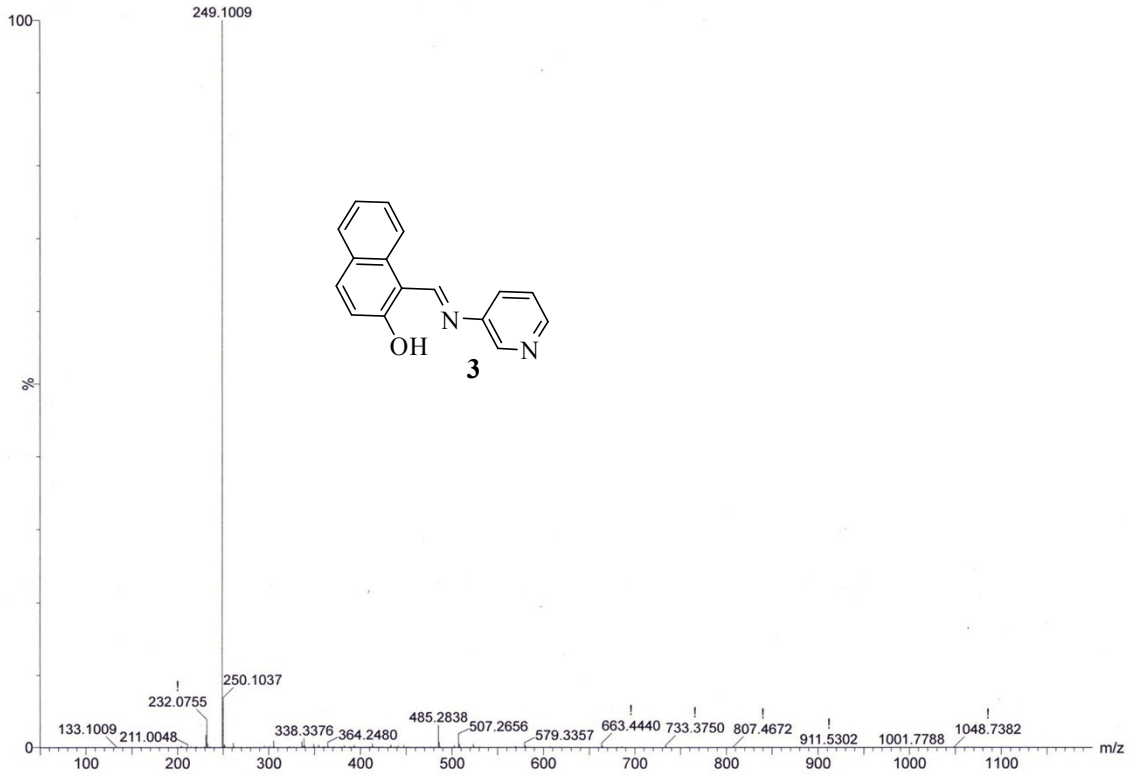

Table 3S. Reported structures for Fe^{3+} sensing in solution and gel phase.

Entry	Gelator structure	Gelation	Sensing mechanism	solvent	Detection limit (M)	Interference from other metal ions	Ref.
1	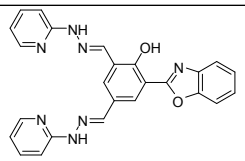	No gelation	Fluorescence OFF	H_2O/ EtOH = 8 : 2	-	Cr^{3+}, Al^{3+}	4a
2	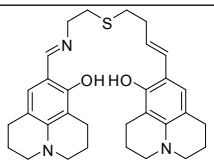	No gelation	Colorimetric sensing	MeOH–buffer solution (9 : 1, v/v, 10 mM, bis-tris, pH 7.0)	2.2×10^{-7}	Fe^{2+}	4b
3	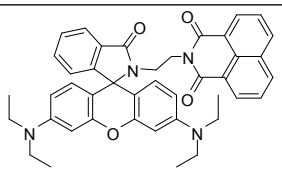	No gelation	Fluorescence ON	MeOH–H2O (6 : 4, v/v, 25 °C, pH = 7.1, 20 mM HEPES buffer)	2.9×10^{-6}	Cr^{3+}, Al^{3+}	4c
4	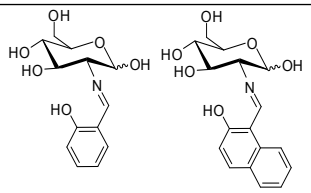	No gelation	Colorimetric sensing	MeOH aqueous HEPES buffer at pH 7.2	5.0×10^{-6} 5.0×10^{-6}	Fe^{2+}, Cu^{2+} Fe^{2+}, Cu^{2+}	4d
5	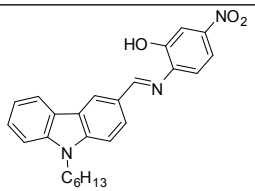	No gelation	Fluorescence ON	CH_3CN	4.23×10^{-6}	Cu^{2+}	4e
6	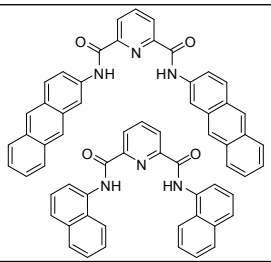	No gelation	Fluorescence OFF	THF	5.56×10^{-6} 6.08×10^{-6}	Fe^{2+}	4f
7	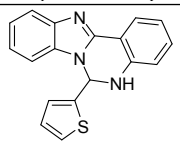	No gelation	Chemosensor	HEPES buffer (100 mM, acetoni-trile : water 1 : 4 (v/v), pH 7.4)	3.5×10^{-6}	-	4h
8	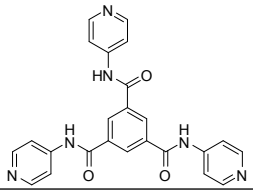	Gelation	Sol to gel transition	Water	-	Fe^{2+}	4i

9	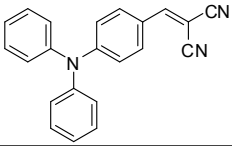	No gelation	Fluorescence OFF	Water containing very little amount of DMSO	1.44×10^{-6}	-	5a
10	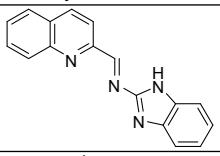	No gelation	Fluorescence ON (CHEF process)	CH_3CN/aqueous HEPES buffer (1 mM, pH 7.3; 1 : 4 v/v)	4.0×10^{-6}	-	5b
11	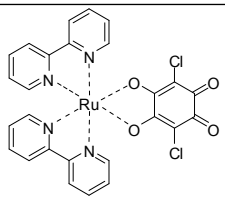	No gelation	Fluorescence ON	CH_3CN/DMF= 7 : 3 v/v	3.3×10^{-6}	Cu^{2+}	5c
12	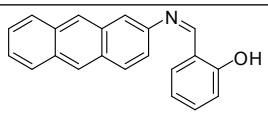	No gelation	Fluorescence ON	THF	2.95×10^{-6}	Fe^{2+}	4g
13	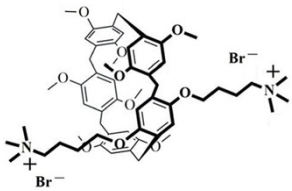	Gelation	Fluorescence OFF	H_2O	7.86×10^{-10}	-	4j
Our work	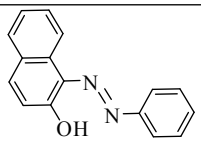 **1**	Gelation	Visual detection through gel-to-sol transition	CH_3CN/ H_2O (1:1)	7.92×10^{-6}	Cu^{2+}	
	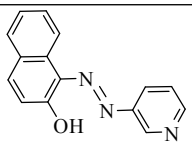 **2**	Gelation	Visual detection through gel-to-sol transition	CH_3CN/ H_2O (1:1)	1.18×10^{-6}	-	
	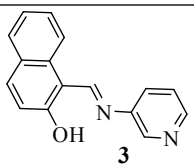 **3**	Gelation	Visual detection through color change Fluorescence ON (CHEF process)	DMSO/ H_2O (1:1) CH_3CN/ H_2O (1:1)	 9.76×10^{-7}	-	

References

1. T. S. B. Baul and D. Deg*, Synth. React. Inorg. Met. -0rg. Chem.*, 1990**, 20**, 541.

2. Z. Khayat and H. Z. –Boeini, *Dyes Pigm.*, 2018**, 159**, 337.

3. (a) A. K. Mahapatra, S. S. Ali, K. Maiti, S. K. Manna, R. Maji, S. Mondal, M. R. Uddin, S. Mandal and P. Sahoo, *RSC Adv.*, 2015, **5**, 81203; (b) T. –B. Wei, P. Zhang, B. –B. Shi, P. Chen, Q. Lin, J. Liu and Y. –M. Zhang, *Dyes Pigm.*, 2013, **97**, 297; (c) H. J. Jung, N, Singh, D. Y. Lee and D. O. Jang, *Tetrahedron Lett*., 2010, **51**, 3962; (d) M. J. C. Marenco, C. Fowley, B. W. Hyland, G. R.C. Hamilton, D. Galindo-Riaño and J. F. Callan, *Tetrahedron Lett*., 2012, **53**, 670.

4. (a) J. Wang, Y. Li, N. G. Patel, G. Zhang, D. Zhoub and Y. Pang, *Chem. Commun.***,** 2014, **50**, 12258; (b) Y. S. Kim, G. J. Park, J. J. Lee, S. Y. Lee, S. Y. Lee and C. Kim, *RSC Adv.*, 2015, **5**, 11229; c) S. Paul, A. Manna and S. Goswami, *Dalton Trans.*, 2015, **44**, 11805; (d) A. Mitra, B. Ramanujam and C. P. Rao, *Tetrahedron Lett*., 2009, **50**, 776; (e) L. Yang, W. Zhu, M. Fang, Q. Zhang and C. Li, *Spectrochimica Acta Part A: Molecular and Biomolecular Spectroscopy*, 2013, **109**, 186; (f) P. Kumar, V. Kumar and R. Gupta, *RSC Adv.*, 2015, **5**, 97874; (g) S. Sen, S. Sarkar, B. Chattopadhyay, A. Moirangthem, A. Basu, K. Dhara and P. Chattopadhyay, *Analyst*, 2012, **137**, 3335; (h) J. –L. Zhong, X. –J. Jia, H. –J. Liu, X. –Z. Luo,S. –G. Hong, N. Zhanga and J. –B. Huang, *SoftMatter*, 2016, **12**, 191; (g) M. Shellaiah, Y. –H. Wu, A. Singh, M. V. R. Raju and H. –C. Lin, *J. Mater. Chem. A*, 2013, **1**, 1310; (h) S. Sen, S. Sarkar, B. Chattopadhyay, A. Moirangthem, A. Basu, K. Dhara and P. Chattopadhyay, *Analyst*, 2012, **137**, 3335; (i) J. –L. Zhong, X. –J. Jia, H. –J. Liu, X. –Z. Luo,S. –G. Hong, N. Zhanga and J. –B. Huang, *SoftMatter*, 2016, **12**,191; (j) J. –F. Chen, Q. Lin, H. Yao, Y. –M. Zhang and T. –B. Wei, *Mater. Chem. Front.*, 2018, **2**, 999.

5. (a) X. Yang, X. Chen, X. Lu, C. Yan, Y. Xu, X. Hang, J. Qu and R. Liu, *J. Mater. Chem. C*, 2016, **4**, 383; (b) C. Kar, S. Samanta, S. Mukherjee, B. K. Datta, A. Ramesh and G. Das, *NewJ.Chem.*, 2014, **38**, 2660; (c) A. K. Singh and R. Nagarajan, *Dalton Trans.*, 2015, **44**, 19786; (e) A. K. Das and S. Goswami, *Sens. Actuators, B*, 2017, **245**, 1062.